Acknowledgements

SUMMARY

INFLUENCE OF A PRE-DEFORMATION ON THE CRITICAL STRAIN FOR THE ONSET OF DYNAMIC RECRYSTALLIZATION OF Ti-Nb MICROALLOYED STEELS

An empirical equation was developed for the prediction of the critical strain for the onset of dynamic recrystallization (DRX) in microalloyed Nb-containing steels. Single-rolling pass isothermal compression tests were carried out in a Gleeble 1500^{TM} thermomechanical processing simulator at 1000, 1050, 1100 and 1150 ^{o}C and strain rates of 0.5, 1 and 3s^{-1}. The strain was 0.85. The Nb content was systematically varied between 0.024 and 0.10 mass %Nb. No further effect of addition of Nb on the critical strain was observed above 0.068%. The double-hit isothermal compression tests were carried out to investigate the influence of retained strain on the critical strain for DRX under the same conditions spelt out above but in tests in which the pre-strain was kept below the critical strain i.e. 0.142, and the amount of retained strain was varied by increasing the inter-pass time from 0.5 s to 8 s. As expected, the introduction of a pre-strain decreased the critical strain for the initiation of DRX. The data obtained from the experimental tests were used to develop an empirical model for the prediction of the critical strain for the onset of DRX taking into account the Nb content and the retained strain. A good correlation was obtained between the predicted and the experimental results.

Keywords: Dynamic recrystallization, retained strain, Nb-Ti microalloyed steels, inter-pass time.

Candidate	:	Mukadi Clovis Mulala
Supervisors	:	Professor Roelf J. Mostert
		Professor Charles W. Siyasiya
Department	:	Materials Science and Metallurgical Engineering
University	:	University of Pretoria
Degree	:	Master of Science (Applied Science) Metallurgy

Publication

TABLE OF CONTENTS

LIST OF FIGURES

LIST OF TABLES

1. INTRODUCTION

1.1. Background

High-strength, low-alloy (HSLA) steels are known for their good mechanical properties such as strength, toughness, formability and weldability in comparison with carbon-containing steels. The strength-to-weight ratio is the important factor in the selection of these steels. They are found in many applications such as oil and gas pipelines, heavy-duty highway and off-road vehicles, construction and farm machinery, industrial equipment, storage tanks, mines and railroad cars, passenger car components [1], bridges, off-shore structures, power transmission towers [2] [3], etc. In HSLA steels, the carbon content is low, which improves formability, weldability and toughness but decreases the strength so that alloying elements have to be added for compensation [4]. The chemical composition of an HSLA steel varies in order to meet specific required properties. In sheet or plate form, the composition is typically 0.05-0.25% C, up to 2.0% Mn, then small quantities of Cr, Ni, Mo, Cu, N, V, Nb, Ti and Zr are added in a variety of proportions [5]. The niobium is used in HSLA steels to refine the grains and to increase the yield strength through precipitation-hardening of niobium carbides [6]. During hot deformation of steel, dynamic recrystallization (DRX) starts taking place when the strain reaches a critical amount ε_c which depends on the material (composition, grain size) and the thermomechanical processing conditions (deformation temperature, strain rate and strain) and is used to indicate the initiation of DRX. In mathematical modelling, the ε_c is a quantity used for the evaluation of hot-rolling mill loads and the evolution of the microstructures [7] and their subsequent mechanical properties [8]. The roughing step during hot-rolling takes place above the nil recrystallization temperature T_{nr} (which is dependent on the chemical composition of the steel, the effective strain applied in each pass, the strain rate, the reheating temperature and the initial austenite grain size D₀). It is a critical temperature in hot-rolling below which complete recrystallization of the austenite no longer occurs, it is inhibited. Deformation below T_{nr} (during finishing) will lead to strain accumulation in the austenite grains (pancaking) which will act as a driving force for the ultimate ferrite nucleation from the austenite-to-ferrite transformation and the grains developed after transformation will be finer. The deformation above T_{nr} (during roughing) results in equiaxed recrystallized grains which can coarsen if there is no further recrystallization [9] [10] [11]. During several passes of deformation, with short inter-pass times, it is possible that neither recrystallization nor recovery will occur, the strain will be accumulated and after some

passes, the ε_c will be reached and the DRX will occur. But if the inter-pass time is relatively long, recovery and recrystallization can occur and the dislocation density will remain low and the ε_c of the following pass might not be reached, thus no DRX will occur [12]. This work focuses on the development of a model that can predict during roughing of hot rolling the ε_c for the initiation of DRX in austenite in Nb-containing HSLA steels, taking into account effects of the retained strain from a prior pass. What is new in this work is the inclusion of the effect of the retained strain in the equation for the prediction of the critical strain for the on-set of DRX.

1.2. HIGH-STRENGTH LOW-ALLOY STEELS (HSLA)

1.2.1. Background

High-strength, low-alloy steels are designed to satisfy the demand for good mechanical properties and better atmospheric corrosion resistance, and to face the social and economic pressures led by the need to produce low-cost, but efficient, materials [13]. The metallurgical success of high-strength, low-alloy steels is due to the addition of microalloying elements that, in association with thermomechanical processing, determine the microstructure through which the mechanical properties are improved. The different mechanisms behind this improvement are the carbonitride precipitation, the grain refinement, the structure strengthening and the precipitation hardening [9]. The ferritic fine microstructure that optimizes strength and toughness simultaneously in HSLA steels is due to the prior "pancaked" austenite grain size, which results from the addition of alloying elements that modify the continuous cooling transformation (CCT) curve [14].

1.2.2. Applications of HSLA steels

The mechanical properties of microalloyed steels can sustain high stresses expected in structures such as oil and gas pipelines, construction and farm machinery, vessels, heavy-duty vehicles, power transmission towers, bridges, off-shore structures, light poles, building beams [15] [9], etc. The combination of different microalloying elements leads to a variety of microalloyed steels that are specifically chosen according to their properties and used to meet specific application requirements such as formability, thickness, corrosion, weldability, strength and weight [16]. The last two characteristics are very important for the automobile component manufacturing industry.

1.3. HOT-ROLLING OF STEELS

1.3.1. Background

Hot-rolling is a plastic deformation process at elevated and controlled temperatures through rotating rollers. For steels, the hot-rolling process is performed in the temperature range of 850-1320 ºC [17]. In the past, hot-rolling used to be a process allowing control of the shape and the dimensions of the slab. There was no need to control the microstructure as the strength requirement was still very low. With the technology evolution, more applications required higher strength; therefore higher mechanical properties had to be achieved. This is facilitated by a small addition of alloying elements for the formation of carbide and/or nitride precipitates and grain refinement that lead to higher strength and toughness of steels. The

improvement in the mechanical properties of steels is one of the major motivations behind different research projects that are being conducted. Focusing on the deformation, researchers confirmed that a double-step rolling process (roughing and finishing) could bring better results. This process is known as a thermo-mechanically controlled process [18].

Initially, the steel ingot is hot-rolled and the size is reduced to produce blooms and billets. Further hot-rolling steps will allow the production of rods, bars, pipes, joints and special profiles, rounds, rails, plates, sheets, etc.

At ArcelorMittal Vanderbijlpark, the slabs (that are coming from the iron-making, followed by the steel-making process) are hot-rolled to 1.5-23mm thick and 750-1850 mm wide. The coils that are produced may be sold or sent for further cold-rolling and coating (hot-dip galvanisation, electro-galvanisation, and pre-painting). The Hot Strip Mill route is composed of four furnaces, a two-stand tandem roughing mill, a seven-stand tandem finishing mill and three coilers. The slab is heated to more or less 1250 ºC, rolled through roughing from 240 mm thick to 30-42 mm transfer bar. The bar obtained is then sent to the finishing stands and coiled. In the Plate Mill Route, the slabs are reheated in furnaces and rolled into heavy plate of 5-10mm thickness and 3500mm width with diverse lengths of plates of which the temperature is decreased on the cooling beds before they are cut and heat-treated in the Treatment Plant for improved steel properties and wear resistance [19].
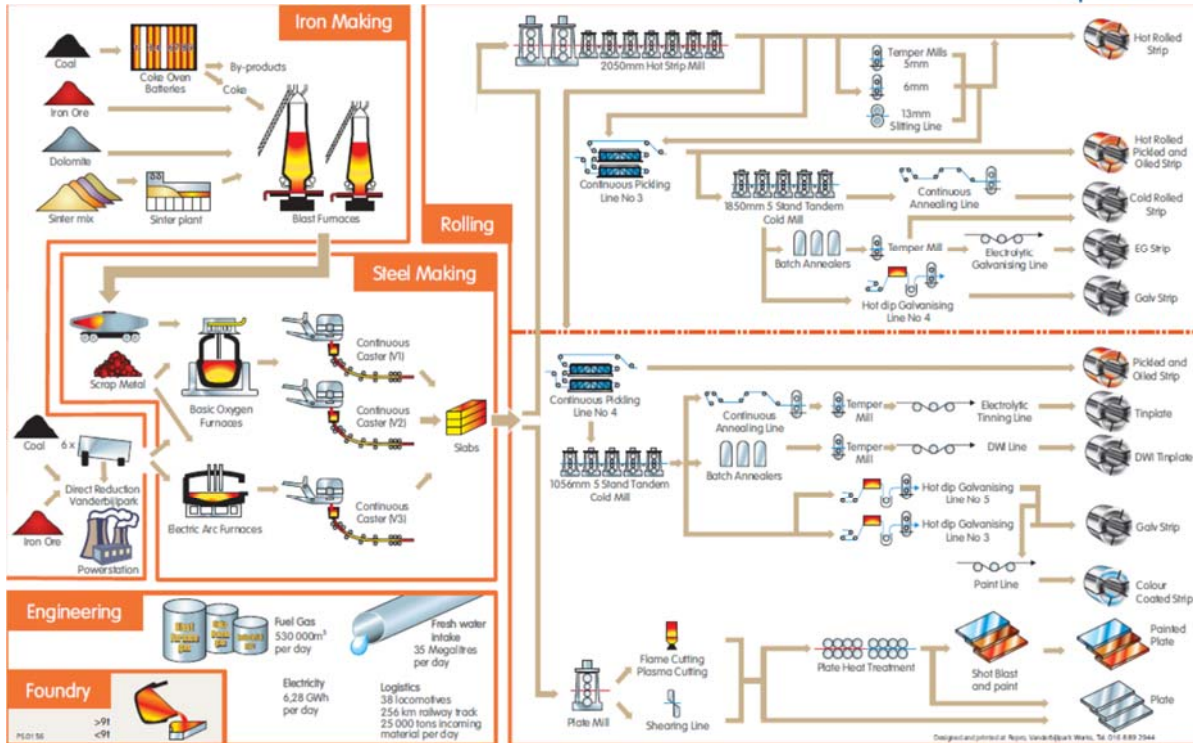
Figure 1.Process flow chart of Vanderbijlpark, Arcelor Mittal South Africa [19]

1.3.2. Thermo-mechanical process

High-strength, good-ductility and low-temperature toughness of steels can be achieved only by refinement of ferrite grains, which is the main goal of the thermo-mechanical processing (TMP) of microalloyed steels [9]. The microalloyed steel is reheated or soaked between 1200 to 1320 ºC, then it is cooled to the deformation temperature for the first step of the TMP (rough rolling) that takes place at high temperatures (above T_{nr}, 1050 to 1250 ºC) where the coarse grains from the cast are refined through dynamic recrystallization. Then the steel is held until the temperature decreases to about 900 ºC, where the second step (finish-rolling) can occur. No recrystallization takes place during the finish-rolling because, it take place below the no-recrystallization temperature. The pancaked austenite grains remain elongated in the matrix. The grain boundary area is greater and because there are more sites for the austenite-to-ferrite transformation as well as high dislocation content, the ferrite nucleation rate is high. That will lead to finer ferrite grains [17] [18].
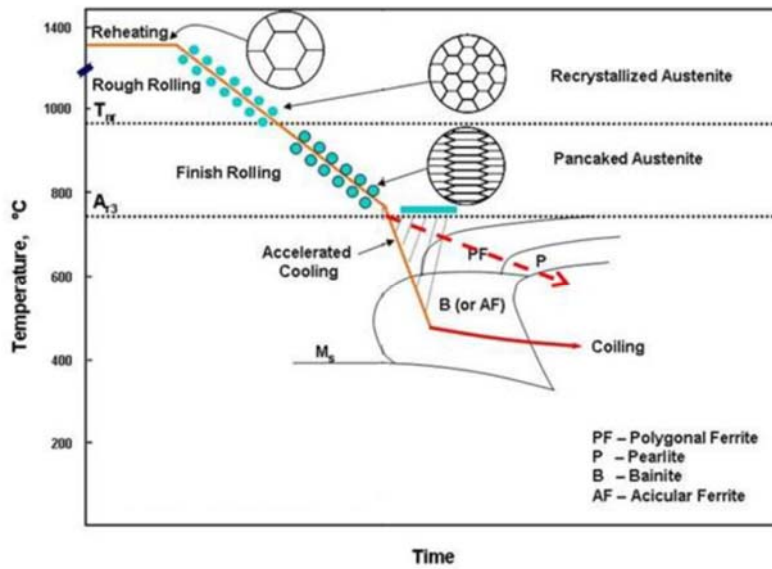
Figure 2. Thermo-mechanical schema of steels with the completion of the recrystallization during rough rolling and pancaking in the absence of recrystallization during finish-rolling [18]

The different mechanisms that take place during the TMP are recovery, recrystallization, precipitation and grain-coarsening, depending on the steel composition, the temperature, the strain, the strain rate and the holding time between consecutive deformation steps.
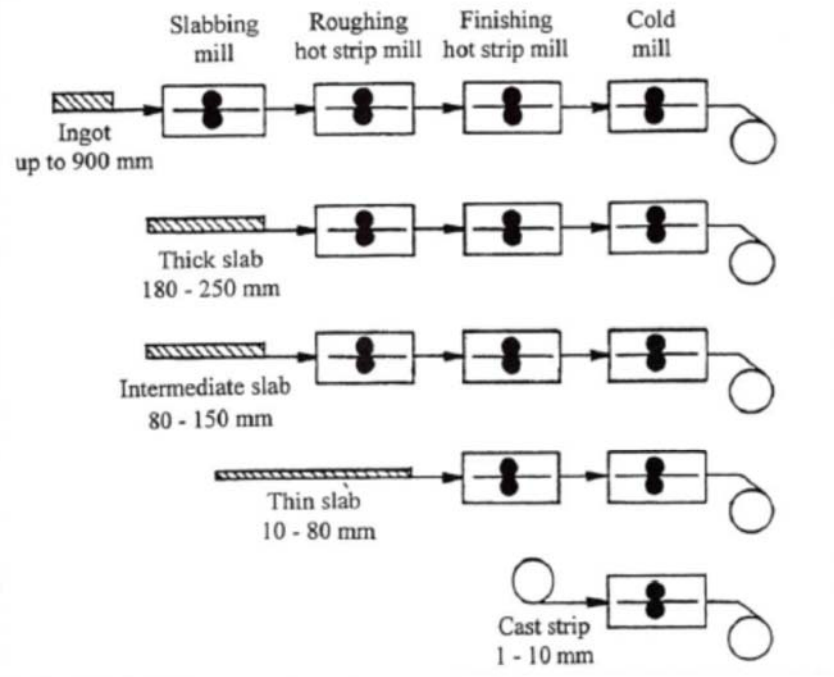
Figure 3. Flow of rolled material through various rolling mills [17]

1.3.3. Problem statement

In hot-rolling, it is beneficial to improve the efficiency and the productivity of a process and the quality of the end product. For microalloyed steels, this can be achieved by using empirical models that can predict the microstructural evolution of the product, given a set of thermomechanical parameters. During roughing of microalloyed steels, it is beneficial for the material to undergo repeated dynamic recrystallization without grain growth. This repeated DRX results in a finer austenitic microstructure that will promote finer ferrite grains in the final product [9] [13]. It is then important to know at which amount of strain the dynamic recrystallization sets in. The available predicting models however, do not consider the effect of retained strain due to successive deformation steps. Taking into account the retained strain effect on the onset of the dynamic recrystallization, this project has the potential to optimize the hot-rolling process of Nb microalloyed steels by studying the influence of Nb content up to 0.10% and the operating parameters (inter-pass time, deformation temperature, strain and strain rate) on the microstructure and the properties of the product (steel).

1.3.4. Objectives

The focus of this project is on hot deformation in the roughing mill where there is a need to predict the critical strain for the onset of DRX, while taking into account the strain that has been retained before the relevant pass. It is of great importance to generate an empirical model that can accurately predict the critical strain (ε_c) for the onset of DRX in HSLA steels containing up to 0.10% Nb. The retained strain is taken into account because this work deals with a multi-pass type of deformation. Such a model will be useful in predicting the hot-working behaviour of the entire typical range of Nb content from low to high Nb for strip steels.

1.3.5. Industrial benefit

A potential benefit of this project is the optimization of the hot-rolling process (roughing) of Nb microalloyed steels by improving the operational efficiency/productivity without compromising the product quality (finer grains).

1.3.6. Research plan

The following variables have been considered to achieve the above objective:

- Chemical composition: the Nb % will be varied while the rest of alloying elements will be kept almost constant.

- Inter-pass time (that will promote the variation of strain accumulation)

- Temperature

- Starting grain size (austenite grain size) D_0

- Strain rate $\dot{\varepsilon}$

2. THEORETICAL FOUNDATION

2.1. Softening mechanisms

2.1.1. Background

Recovery, recrystallization and grain growth are the three processes or softening mechanisms that can lower the free energy stored in the steel in the form of dislocations (Figure 5). This energy is increased in the material due to deformation. During recovery, the dislocation density is lowered by annihilation and rearrangement. Recrystallization takes place when new grains free from dislocations, nucleate in the steel. The grains from the original structure will dissolve and leave space for the new grains with much reduced dislocations. When these new grains become larger, the amount of grain boundary surface area decreases through grain growth. The mechanisms operating during the softening processes depend on the hot-rolling conditions and the material's chemistry [20].
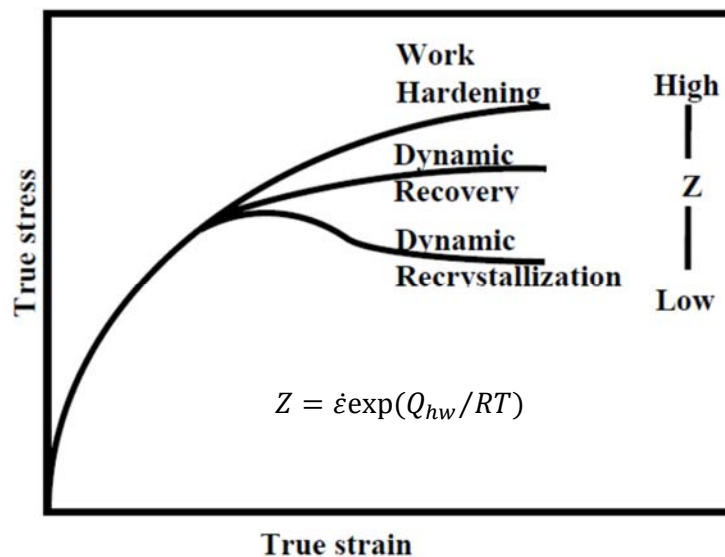
Figure 4. Illustration of work-hardening, dynamic recovery and dynamic recrystallization during hot deformation [21]

The flow curve (Figure 4) depends on the deformation conditions which are mainly the temperature and the deformation rate $\dot{\varepsilon}$ of which the Zener-Hollomon parameter Z is the practical expression. It is also called the temperature-compensated strain rate parameter. The material that is being deformed undergoes work-hardening when the Z value is very high, dynamic recovery when the Z value is average and dynamic recrystallization when the Z

value is low (Figure 4). The Z value is heavily dependent on the deformation activation energy Q_{hw}.

$$Z = \dot{\varepsilon}\exp(Q_{hw}/RT) \tag{1}$$

where, Q_{hw} is the activation energy for deformation, $\dot{\varepsilon}$ the strain rate, $R=8.314\ J/mol\ K$ the gas constant and T the absolute temperature.
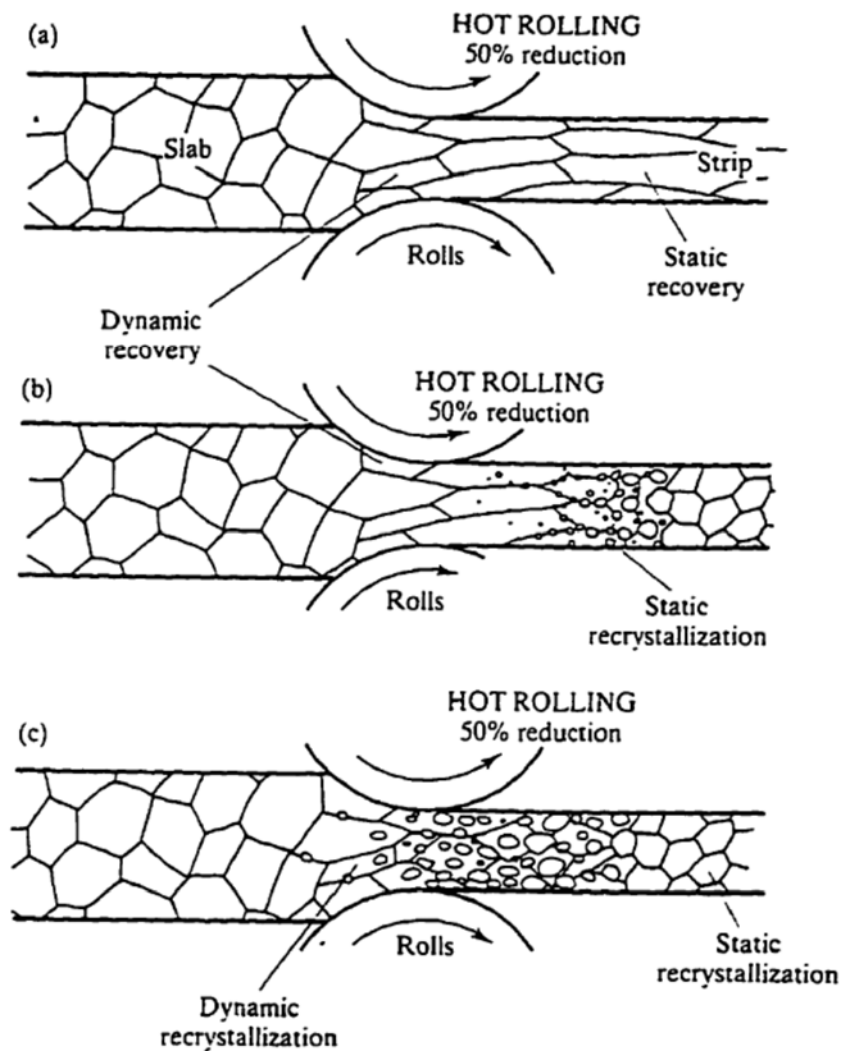
Figure 5. Schematic of possible microstructural changes during hot deformation [22]

2.1.2. Recovery

The free energy stored in the material in the form of higher dislocation density (due to strain) and a higher number of grain boundaries act as a driving force for recovery. This energy is lowered by a rearrangement of dislocations. Still due to deformation which implies the motion of dislocations, there is formation of cells, and within these, dislocation annihilation takes place [21]. These cells become subgrains of which the boundaries are regions of high dislocation density (Figure 4). These subgrains grow later. All these phenomena occur within the original grain; there are no new grains. When this process occurs during hot deformation, the metal undergoes a dynamic recovery.

(a) Dislocation tangles   (b) Cell formation   (c) Annihilation of dislocations within cells

(d) Subgrain formation   (e) Subgrain growth
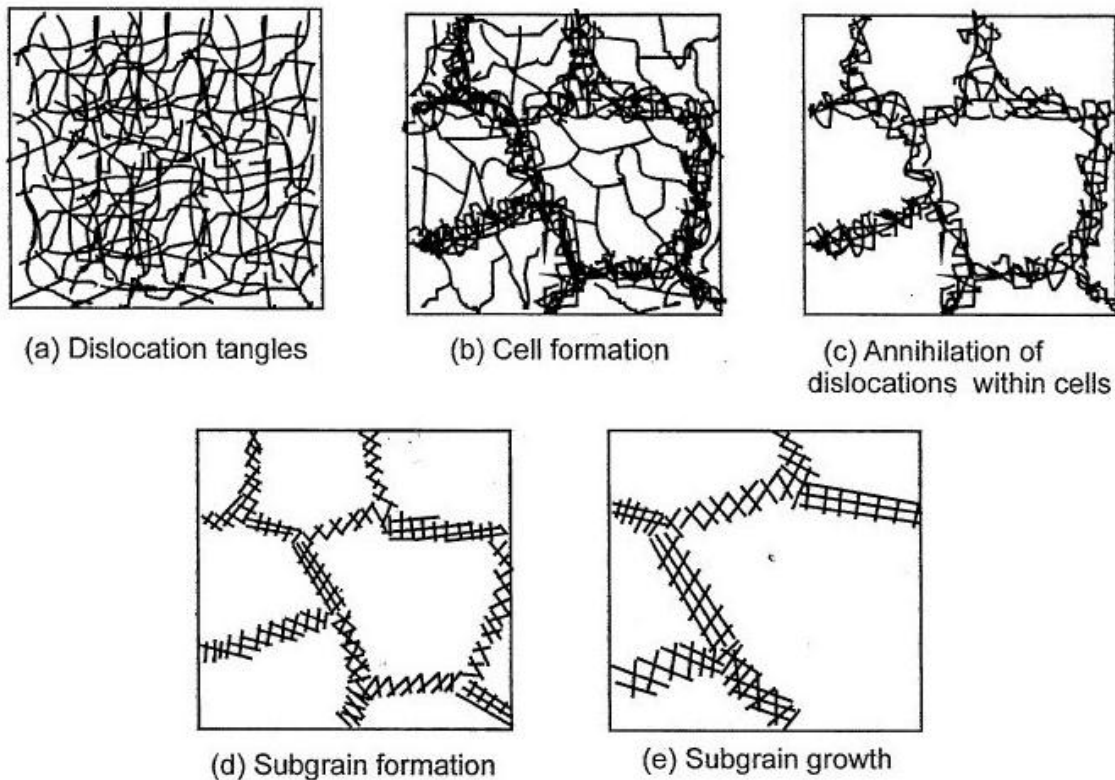
Figure 6. Different stages where the rearrangement of dislocations leads to subgrain formation and growth [21]

During hot deformation, there is an increase in dislocation density that can compete with the annihilation and the rearrangement of dislocations. Hence the evolution of dislocation density ρ can be described as follows:

$$\frac{d\rho}{dt} = \frac{d\rho_{gen}}{dt} - \frac{d\rho_{recov}}{dt}$$

(2)

11

where, ρ_{gen} and ρ_{recov} are the densities respectively of the generated dislocations (due to deformation) and annihilated or rearranged dislocations (due to recovery).

When the recovery and the work-hardening occur at the same rate, the flow curve will show a plateau, with the recovery being the main softening mechanism, through a process known as dynamic recovery (DRV).

The change in ρ due to static recovery depends on the chemical composition, the deformation conditions and time after deformation. When the specimen is deformed and then held at high temperature, the recovery takes place by climbing of dislocations and when the deformation and holding temperatures are low, the recovery takes place by annihilation of dislocations of opposite Burgers vectors or incorporating of dislocations into cell walls. Recovery is retarded by a decrease in deformation and holding temperatures and an increase in Nb% [23].

2.1.3. Recrystallization

The recrystallization is a softening mechanism that a work-hardened metal undergoes during the annealing process. A nucleation driven phase transformation occurs during this softening process, driven by a lowering of the free energy. The nucleation and the growth of new grains take place during recrystallization. The new grains in the structure are formed by the migration of high-angle grain boundaries (HAGBs). In fact, the subgrains with higher misorientation will grow faster than those with low orientation angles and will lead to the nuclei formation for recrystallization [21] [24]. It is driven by the energy that has been stored in the metal during deformation by increasing the dislocation density. The nucleation and growth can take place preferentially along the prior austenite grain boundaries but when the deformed grains are large, the nucleation can occur within the prior austenite grain (Figure 7).

2.1.3.1.   Driving force for recrystallization

When the metal is being deformed, the dislocations are multiplied by several mechanisms, and some atoms are no longer at their equilibrium position where their free energy is the lowest. The elastic energy is stored in the form of dislocations, and is a function of the Burgers vector [25] [26].

$$E_{el} = 0.5 \, G_M b^2 \tag{3}$$

where G_M is the elastic shear modulus in MPa, b the Burgers vector and E_{el} the elastic energy per unit length of the dislocation line.

The total stored energy in the metal is calculated by multiplying the energy per unit length by the length of all the dislocations per unit volume formed during the deformation.

$$E_{tot} = 0.5\ G_M b^2 (\rho_{d_f} - \rho_{d_0}) \tag{4}$$

where, ρ_{d_f} and ρ_{d_0} are respectively the dislocation density after and before the deformation.

$$\text{But,} \quad \rho_{d_f} \gg \rho_{d_0}$$

$$\text{Hence,}\ E_{tot} \approx 0.5\ G_M b^2 \rho_{d_f}$$

After the recrystallization process, the number of dislocation is decreased to close to that before the deformation and the stored energy decreases to steady state. This is why the total elastic strain energy is considered to be the driving force for the recrystallization and the interface of the new grain which is forming is a retarding force with the energy (γ_{SF}). The free energy equation [26] [25] will be:

$$\Delta G = \underbrace{V \Delta G_v}_{-} + \underbrace{A \gamma_{SF}}_{+} \tag{5}$$

$$\Delta G = (4/3)\pi r^3 (0.5 G_M b^2 \rho_d) + 4\pi r^2 \gamma_{SF} \tag{6}$$

At high strain, the number of dislocations is very high, there is more driving force and the nucleation of new grains is easier and faster because of lower activation energy and a higher nucleation rate. The new recrystallized grains grow from the nuclei that have enough energy (high-angle boundary) and a large enough size. This is the critical size that can be reached only when there is an abnormal growth of a previous subgrain [21].

$$r^* = -\frac{2\gamma_{SF}}{0.5 G_M b^2 \rho_d} \tag{7}$$

$$\Delta G^* = -\frac{16\pi \gamma_{SF}^3}{0.5 G_M b^2 \rho_d} \tag{8}$$

$$\dot{N} = K_1 exp\left[-\frac{Q + \Delta G^*}{RT}\right] \tag{9}$$

where, r^* is the critical size (radius) of a nucleus that can grow, ΔG^* is the activation energy for the nucleus to form, γ_{SF} the surface energy, $\dot{N}$ the nucleation rate, Q the self-diffusion rate in the metal and K_1 a material constant.
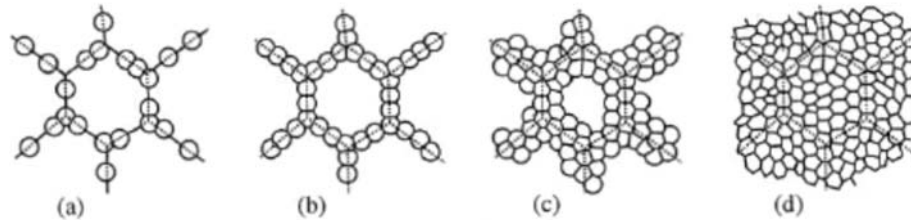
Figure 7. Development of recrystallizing grains where the prior austenite grain is large. The prior austenite grain is represented by the dotted lines [21].

The softening process is called static recrystallization (SRX) when this microstructural change occurs after the hot deformation and it is called meta-dynamic recrystallization when the softening mechanism continues after deformation during which DRX had already taken place [21] [27].

2.1.4. Dynamic recrystallization

Dynamic recrystallization (DRX) is a softening process during hot deformation of steels where the grain boundaries are continuously rebuilt and is a very important process in microstructure control [28] [29]. The microstructural changes brought about by the DRX during hot deformation lowers the hardness of the metal [27]. It takes place when the strain reaches a critical amount of deformation. New grain nucleation occurs and the new grains grow while deformed grains are being dissolved.

2.1.4.1. Initiation of DRX

This nucleation of new grains requires a critical density of dislocations. It can also be expressed as the critical strain (associated with the critical stress) for the initiation of DRX. The critical strain on the stress-strain curve indicates the start of dynamic recrystallization. When the steel is deformed, its microstructure is transformed by work-hardening and multiplication of dislocations which will set the conditions for the nucleation and growth of new grains. There will be softening competing with hardening in other regions in the matrix. Then the work-hardening rate will decrease until the peak stress is reached, where the softening mechanism becomes more important [30]. The critical strain is a fraction of the

peak strain and indicates the onset of the DRX [31]. At low temperature, there might not be a pronounced peak strain but it does not necessarily mean that DRX has not initiated [32] [33].

2.1.4.2.   Equations for the critical strain for the onset of the DRX

The literature proposes several equations that can be used to predict the initiation of DRX. They are as follows:

$$\varepsilon_c = AD_0^m Z^q \tag{10}$$

where, ε_c is the critical strain for the onset of dynamic recrystallization, D_o the austenite grain size, Z the Zener-Hollomon parameter, m and q material constants, and A the structural factor. Sometimes, the critical strain is given as a fraction of the peak strain (ε_p).

In their work, MA Liqiang et al. [34] investigated the DRX behaviour of Nb-Ti microalloyed steels by isothermal single compression tests. A retardation of DRX and an increase in peak strain were observed because of the precipitation of Nb and Ti carbonitrides.

An equation was developed to express the hot-working activation energy as a function of Nb and Ti in solution.

$$Q_{def}(kl/mol) = 267 - 85[C] + 48[Si] + 65[Mn] + 550[Nb]_{eff1}^{0.6} \tag{11}$$

where, $[C]$, $[Si]$ and $[Mn]$ were respectively the weight % of carbon, silicon and manganese content, and $[Nb]_{eff1}$ the effective niobium content which was determined as follows:

$[Nb]_{eff1} = [Nb] + 0.33[Ti]$ because experimentally, the amount of 0.033 wt% Nb produced the same dragging effect as that of 0.1 wt% Ti. [Nb] and [Ti] represented respectively niobium and titanium content.

The structural factor A was expressed by:

$$A = \left(1.42 + 25[Nb]_{eff1} + 4.61[Nb]_{eff1}^{0.6}\right) * 10^{-4} \tag{12}$$

and

$$\varepsilon_c/\varepsilon_p = 0.8 + 7.21[Nb]_{eff1} - 2.25[Nb]_{eff1}^{0.4} \tag{13}$$

15

In their work, F. Siciliano and J. J. Jonas [6] examined the precipitation of Nb carbonitrides which influences the rolling behaviour of Nb steels by preventing softening between passes. Increasing the % Mn reduces the precipitation of Nb, while Si promotes it. The critical strain/peak strain ratio tends to decrease with the addition of Nb content. Mn and Si contents act marginally but opposite on this ratio. The DRX takes place during the first passes due to high strains, low strain rates and high temperatures but in the final passes, it is due to the accumulation of strain.

They reported that the effect of Nb, Mn and Si was considered in an investigation and a fit was found for the critical strain/peak strain ratio. The equations used in that work are:

$$\varepsilon_p = \{(1 + 20Nb)/1.78\} * 2.8 * 10^{-4} * D_0^{0.5}\{\varepsilon * \exp(375000/RT)\}^{0.17} \tag{14}$$

$$\varepsilon_c/\varepsilon_p = 0.8 - 13Nb_{eff} + 112Nb_{eff}^2 \tag{15}$$

Here,

$$Nb_{eff} = Nb - \frac{Mn}{120} + \frac{Si}{94} \tag{16}$$

The equations of the ratio ($\varepsilon_c/\varepsilon_p$) and that of Nb effective are valid for the following ranges: 0.010-0.058% Nb, 0.35-1.33% Mn, and 0.01-0.23 %Si.

Yun Bo Xu et al. [8] investigated the microstructural evolution of high-Nb HSLA steels during mechanical processing. Single- and double-hit tests, as well as isothermal-deformation-quenching tests were performed to quantify the constitutive behaviour, the recrystallization and the precipitation. An expression of the critical strain for DRX was developed for a Nb content up 0.1%.

The equation of the ratio $\varepsilon_c/\varepsilon_p$ proposed by Sicliano and Jonas is valid for only low Nb content steels (≤ 0.06%) but Yun Bo Xu et al. established another equation capable of fitting a wider range of Nb content up to 0.1%.

$$\varepsilon_c/\varepsilon_p = 0.8 - 10.8Nb_{eff} + 64.4Nb_{eff}^2 \tag{17}$$

$$Nb_{eff} = Nb - \frac{Mn}{120} + \frac{Si}{94} \tag{18}$$

16

Soheil Solhojoo and Ebrahimi in their work [35] developed an algorithm to simulate the flow stress curves for multi-pass hot-deformation processes. Single-pass hot-torsion tests on Nb-microalloyed steels provided the data which were used.

In order to study the softening mechanism, they calculated the critical strain for the onset of DRX by using the following equations:

$$\varepsilon_c = B.\varepsilon_p \tag{19}$$

$$B = 0.8 - 10.8[Nb_{eff}] + 64.4[Nb_{eff}]^2 \tag{20}$$

$$Nb_{eff} = Nb - \frac{Mn}{120} + \frac{Si}{94} \tag{21}$$

$$\varepsilon_p = \left(\frac{1 + 20Nb_{eff}}{6360}\right) D_0^{0.5} Z^{0.17} \tag{22}$$

2.1.5. Critical temperatures

There are important critical temperatures that are reached in the hot-working process of HSLA steels which need to be taken into consideration at every step of the process.

2.1.5.1. *Nil recrystallization temperature*

With reducing temperature during hot-rolling, the first critical temperature to be reached is the nil recrystallization temperature (T_{nr}). Above this temperature, the steel can experience complete recrystallization (Figure 8a). If the steel is held below this temperature, it will no longer undergo a complete recrystallization (Figure 8 b) while the austenite experiences work-hardening due to strain accumulation [17] [35] [36]. Empirical equations or laboratory methods such as the multistep deformation test, double-hit deformation test, stress relaxation test, or tension compression test have been used to determine the T_{nr}.

Empirical equations

The literature provides many equations to determine the T_{nr} taking into account the deformation conditions and the alloying elements of the steel. These equations do not necessarily apply universally.

Boratto:

$$T_{nr} = 887 + 464C + \left(6445Nb - 644\sqrt{Nb}\right) + \left(732V - 230\sqrt{V}\right)$$
$$+ 890Ti + 363Al - 357Si \tag{23}$$

Bai (original and revised):

$$T_{nr} = 174\log[Nb\left(C + \frac{12}{14}N\right)] + 1444 \tag{24}$$

$$T_{nr} = \beta\, e^{-0.36\varepsilon} \tag{25}$$

Fletcher (original and revised):

$$T_{nr} = 849 - 349C + 676\sqrt{Nb} + 337V \quad (R^2 = 0.72) \tag{26}$$

$$T_{nr} = 203 - 310C - 149\sqrt{V} + 657\sqrt{Nb} + 683e^{-0.36\varepsilon} \tag{27}$$

where, C, Nb, V, Ti, Al, Si are the alloying element contents in wt. % and N the free nitrogen remaining after the TiN precipitation in the steel, β an alloy-dependent coefficient and ε the strain [17] [36].

2.1.5.2. Recrystallization stop temperature and Ar₃

Below the non-recrystallization temperature (T_{nr}), there is the recrystallization stop temperature (T_r) from where no form of any recrystallization at all can take place (Figure 8 c). This critical temperature (T_r) is reportedly to be about 75 ºC below the (T_{nr}). Then the austenite transforms into ferrite at even a lower temperature which is known as the Ar3 temperature [17] [37].
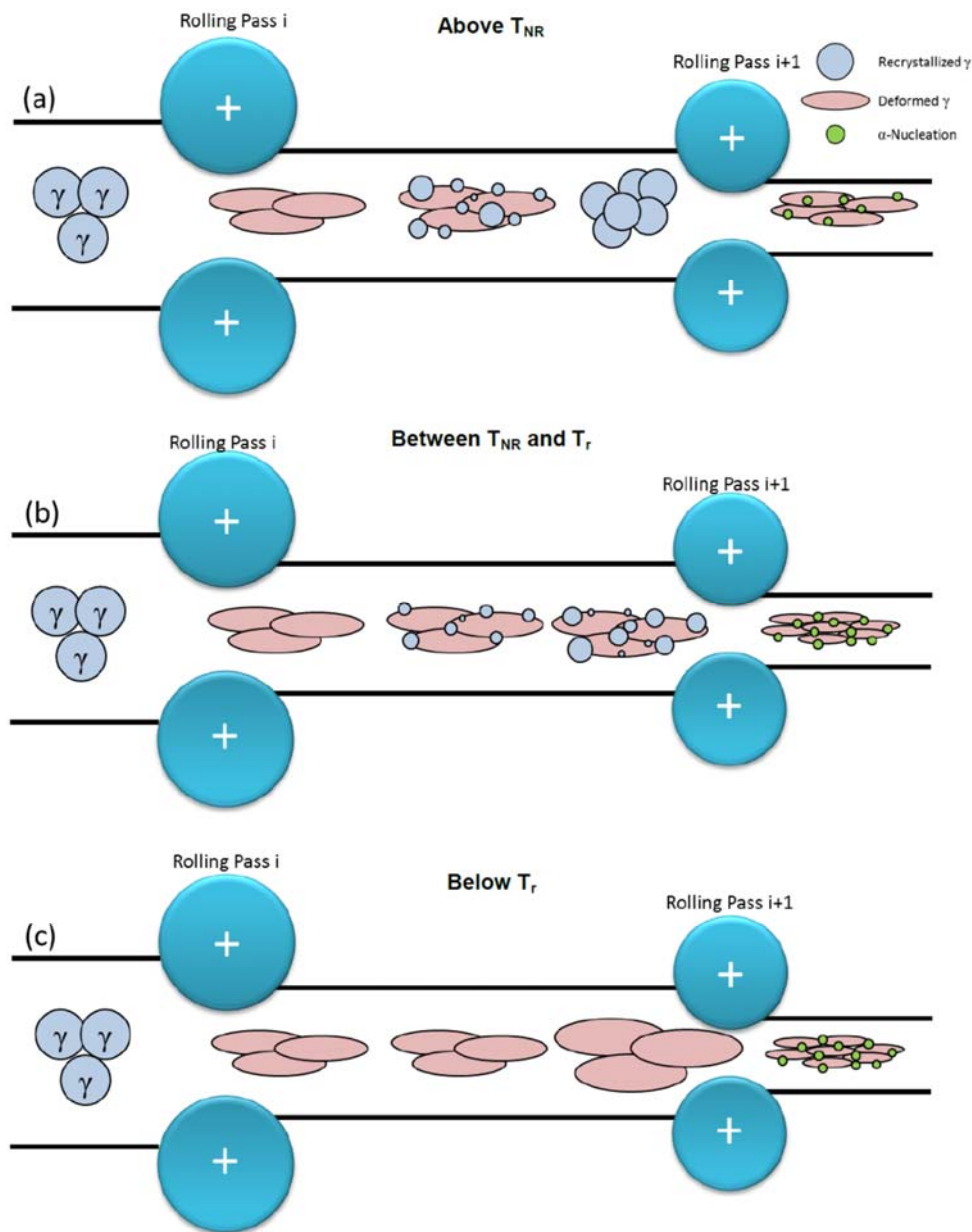
Figure 8. Schematic illustration of deformation (a) above T_{nr}, (b) between T_r and T_{nr} and (c) below T_r [17]

2.2. Strengthening mechanisms

2.2.1. Background

Mechanical properties of steels can be improved by controlling the microstructure. Many methods can be used such as solid-solution strengthening, work-hardening, precipitation-hardening, grain boundary strengthening (grain refinement) to hinder the motion of multiplied dislocations (during deformation) which leads to strengthening and hardening of

the steel [27]. The strengthening of HSLA steels is made possible by a combination of grain refinement, precipitation hardening and solid-solution strengthening [38]. Grain refinement is the most efficient way to increase both strength and ductility of microalloyed steels. It is made possible through the addition of microalloying elements [38] such as Nb, or Ti. The grain growth is restricted by the TiN precipitates and Nb retards the austenite recrystallization by precipitates pinning the boundary (Nb carbonitrides) [4]. The particles that nucleate in the ferrite are more responsible for strengthening [39]. In the austenitic matrix, the fine precipitates restrain the motion of dislocations and the sub-structure is stabilized, hence the recrystallization is retarded [13]. The solutes impede the motion of the grain boundaries and retard recrystallization. The steel can also be strengthened by the solute drag effect of Nb atoms in solid solution in the austenite matrix [4] [39] where the dislocations are to some extent hindered in moving. Dislocation rearrangement is hindered, hence there is no recovery, and sub-cells cannot form nuclei for recrystallization [13]. When recrystallization is hindered, there is more accumulation of strain that will finally lead to more driving force and a higher nucleation rate for austenite-to-ferrite transformation, thus finer ferrite grains that give higher strength and toughness.

2.2.2. Solid-solution strengthening

There are two types of solid solution in the crystalline structure of the material. It can be an interstitial solid solution where the alloying elements' atoms (solute) occupy the spaces between the matrix atoms in the lattice or a substitutional solid solution where the atoms of the matrix are replaced in the lattice by the alloying elements' atoms. According to the solute atom size in solution, there is a formation of a stress field (compression or tensile) that will counteract the motion of dislocations, thus increasing the yield strength of the steel [5] [27].

$$\Delta\tau = G_M b \varepsilon^{2/3} c^{1/2} \tag{28}$$

where ($\Delta\tau$) is the required shear stress to overcome the barriers, (G_M) the shear modulus, (b) the Burgers vector, (ε) the lattice misfit strain between the solute and the solvent and (c) the solute atomic concentration.

2.2.3. Work-hardening

During deformation, steel becomes harder and stronger due to the difficulty of multiplied dislocations to move through the matrix as its density is continuously increased. For higher dislocation densities, greater stress will be required for further deformation [27] because the resistance to the motion of dislocations meeting each other [5].

$$\Delta\tau \propto G_M b \rho^{1/2} \tag{29}$$

where $(\Delta\tau)$ is the required shear stress to overcome the barriers, (G_M) the shear modulus, (b) the Burgers vector and (ρ) the dislocation density.

2.2.4. Grain refinement

Grain boundaries are the regions where the continuity of a crystalline structure is interrupted. It is impossible for the dislocations to move through these regions. With small grains, the number of boundaries is high; hence there are more barriers to dislocation motion. More boundaries increase the yield strength of the steel [5] [27]. Grain refinement (Figure 9) is the only way through which the steel becomes more ductile, stronger and tougher at the same time [40]. The Hall-Petch equation expresses this concept as follows:

$$\sigma_{ys} = \sigma_i + k_y D^{-1/2} \tag{30}$$

where, (σ_{ys}) is the flow strength, (σ_i) the overall resistance of the lattice to the dislocation motion which is also known as the friction stress, (k_y) the Hall-Petch constant or locking parameter measuring the contribution of the grain boundary hardening and (D) the grain size.
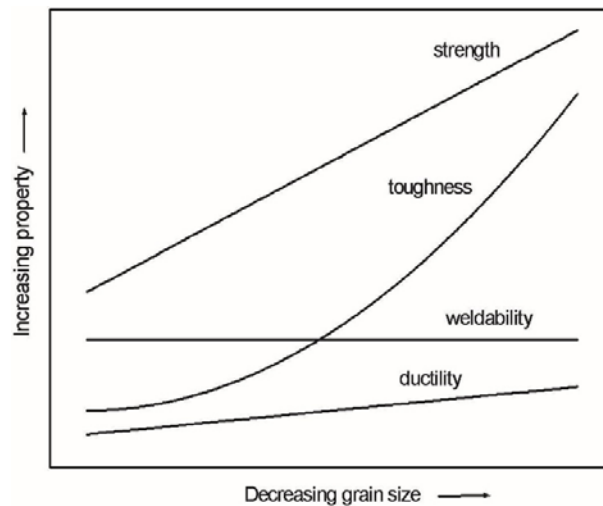
Figure 9. Effect of grain size on processing or mechanical properties [5]

2.2.5. Precipitation strengthening

Dislocation motion is hindered by second-phase particles residing on the slip plane [5]. The strengthening promoted by the precipitates depends on the size of the particles, as well as on their volume fraction. For a fixed volume fraction, the strengthening effect is greater when the particles are smaller i.e., when the number density of particles is high. It is clearly expressed by the Orowan-Ashby model [41]:

$$\sigma_p = 0.538 G_M b \frac{f^{1/2}}{X} \ln\left(\frac{X}{2b}\right) \tag{31}$$

where, (σ_p) is the yield strength increase in MPa, (G_M) the shear modulus in MPa, (b) the Burgers vector in mm, (f) the particle volume fraction, and (X) the real diameter of the second phase particles in mm.

2.3. Alloying elements' effects

2.3.1. Background

The aim of the variation of the chemistry of HSLA steels is to obtain specific mechanical properties. The carbon content goes up to 0.25% while that of manganese can reach 2.0%. The carbon content in HSLA steels is low for good weldability and toughness at the expense of strength but fortunately it is kept high by adding a very small amount of other alloying elements (chromium, nickel, molybdenum, copper, nitrogen, vanadium, titanium, niobium, etc.) in various proportions [16] [17]. The focus on the microalloying elements in this study is directed towards Nb, Ti and V which can retard the recrystallization process and control the austenite grain size by a solute drag effect (dissolved in the matrix) or by precipitation-pinning (nitride and/or carbide precipitates) during the rolling process [42].

2.3.2. Niobium effects

Niobium is known not only for its capability to keep austenite grains at small size but also for its strengthening contribution to the steels by carbonitride precipitation. Niobium has many advantageous effects on microalloyed steels such as reduction of free-carbon in solution in the austenite and increasing the steel strength. As shown in Figure 10, L. Backë observed in her work that the addition of Nb to a C-Mn steel at a certain temperature and a strain rate of 0.1/s led to a retardation in reaching the peak strain (or peak stress which is an indication of the occurrence of DRX) [42], it therefore delays the occurrence of dynamic recrystallization [43]. Although Nb is a ferrite stabilizer, it can be responsible of the austenite-to-ferrite transformation's retardation by the solute drag effect on the phase boundary motion [17].
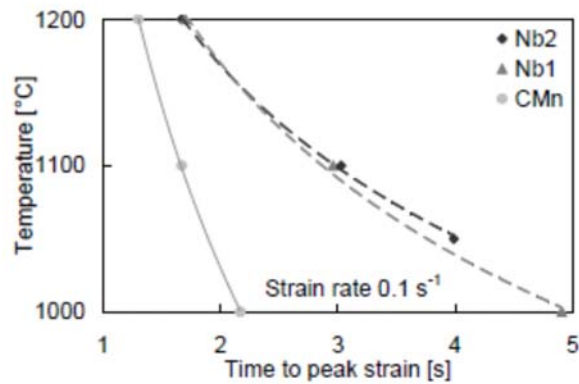
Figure 10. Effect of Nb on the time to reach the peak stress. Nb 2 (0.055%Nb), Nb 1 (0.034%Nb) and C-Mn (0%Nb) [42]

The Nb effect in solution retards the (dynamic and/or static) recovery and the recrystallization as a solute drag [39]. The other effect is that of a precipitate former. The presence of the precipitates will raise the work-hardening and lead to a higher flow stress [44].

Depending on its precipitates' size and their amount, the Nb has an increasing effect on the yield strength through precipitation hardening (Figure 11). It also promotes finer [1] and more acicular ferrite grains due to the pinning effect on the austenite boundaries. This refinement allows a yield strength increase [45]. Nb addition increases the flow stress due to the solid solution and the precipitation during the process (reheating and rolling) [46]. Hence, Nb increases the material strength by promoting finer ferrite grains due to austenite grain refinement.
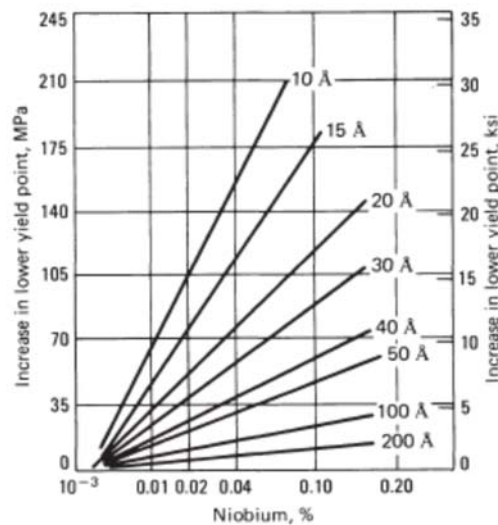
Figure 11. Effect of Nb on the yield strength for various sizes of Nb precipitates [16]

2.3.3. Titanium effect

Titanium plays an important role in reducing the harmful effect of "free" elements such as oxygen, nitrogen, carbon and sulphur by forming stable compounds at high temperatures. It is not really used as a deoxidiser, because it is more expensive than Al which plays this role well [41]. Titanium has a very strong affinity for the formation of nitrides that can have a strong pinning effect when well dispersed with fast enough cooling. This pinning effect can be lowered by long soaking times that allow the coarsening of the nitride precipitates [17]. Ti controls the grain growth at high reheating temperatures as it difficultly goes into solution [47]. Ti addition improves the hot ductility in Nb-containing steels with %C in the peritectic range [48] and also enhances the impact toughness because of the ferrite grain refinement [49]. The titanium carbides prevent the occurrence of the MDRX [50].

2.3.4. Vanadium effect

Vanadium forms precipitates of V(CN), depending on the cooling rate after the hot-rolling schedule of the steel. These precipitates are not stable at typical rolling temperatures, they contribute to the strengthening of ferrite (final steel product) at lower temperatures by pinning grain boundaries [16] [17] [41]. The precipitates are more effective when they are small because of a high enough cooling rate (about 170 ºC/min) (Figure 12). The addition of V in a Ti-Nb microalloyed steel has an improving effect on the product's ductility [48].
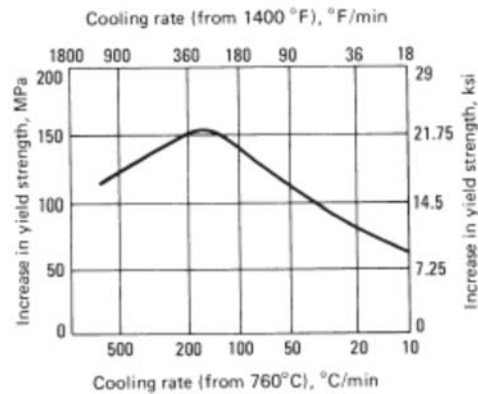
Figure 12. Cooling rate effect on the yield strength due to precipitation strengthening in a 0.15% V steel [16].

Vanadium in solution has a retarding effect on the austenite recrystallization [44].

2.3.5. Boron effect

Boron atoms segregate to the boundaries of austenite grains (Figure 13) and decrease the grain boundary energy which leads to a reduction of the ferrite nucleation rate, thus increasing the hardenability. These atoms occupy interstitial positions and reduce the jump frequency of carbon atoms, retarding again the nucleation of ferrite on austenite grain boundaries. The number of nucleation sites for ferrite is also reduced by the addition of boron atoms [41].
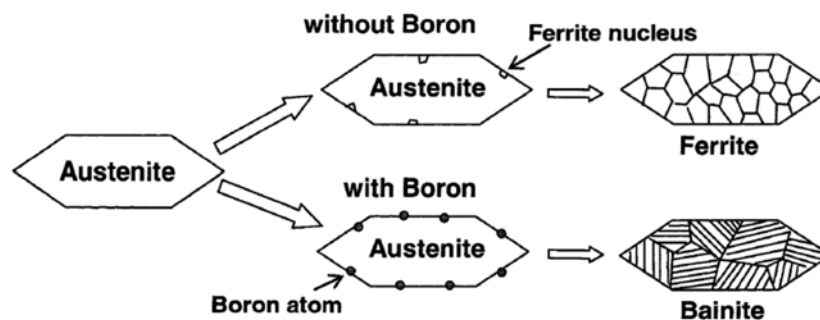
Figure 13. Illustration of the retardation effect of boron on the ferrite nucleation [41]

2.3.6. Carbon effect

The addition of carbon decreases the weldability and the toughness of HSLA steels [16]. It lowers the peak strain in hot working, and decreases the work-hardening and the flow stress,

as well as the peak stress and the deformation activation energy of carbon steels. The carbon content in the steel increases the strength while the ductility is lowered. But in Nb-containing HSLA steels, the addition of C promotes the occurrence of dynamic recrystallization [46]. The carbon content is usually relatively low in HSLA steels because it would compromise the material's ductility.

2.3.7. Manganese effect

Mn additions retard (Figure 14) the precipitation of Nb (CN) and increase the solubility of carbides. The addition of Mn shifts the start and end precipitation curves of Nb (CN) towards the right on the CCT diagram (Figure 14) and therefore, delays the precipitation. Increasing the Mn concentration in Nb-containing microalloyed steels allows an increase in the yield strength of about 1.3% per 0.1 atomic percent of Mn added [44]. Mn has an opposite effect on the carbonitride precipitation compared to that of Si, which increases the precipitation kinetics [6].
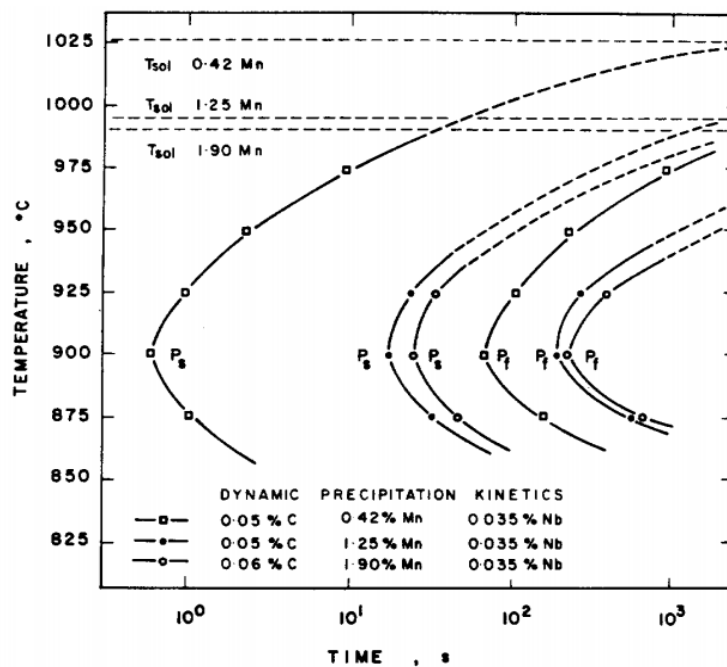
Figure 14. Precipitation time temperature curves for the dynamic precipitation of Nb (CN) in Nb steels [44]

3. EXPERIMENTAL PROCEDURE

3.1. Introduction

This section provides details of the material's characterization and preparation, the experimental equipment used, the experimental procedures that were followed for different tests, and the treatment of data from experiments for the development of an empirical hot working model.

3.2. Material and equipment

3.2.1. Material's characterization

3.2.1.1. Chemical composition

The chemical composition of the high-strength low-alloy steels used in this work is given in *Table 1*. These samples were picked from industrial HSLA steels at the exception of the K66 which was a lab cast steels. The aim was to have a variation of Nb content and keep other alloying element contents constant. It has not been easy since the samples were not lab prepared but accepted "as is". The Nb content was more significantly varied as its influence was to be taken into account. The N, S, B and Ca contents are given in ppm.

Table 1. Chemical composition of studied specimens

ID	grade	Size	C	Mn	Si	Nb	Ti	Cr	Ni	Cu	N*	S*	P	Al	B*	Ca*
S5	HTP	10X5	0.03	1.6	0.20	0.100	0.010	0.2	0.10	0.20	39	80	0.019	0.04	1	0
S4	RC7-01	10X5	0.03	1.5	0.20	0.068	0.011	0.3	0.0	0.0	53	17	0.015	0.07	1	17
S3	RC1-20	10X5	0.07	1.4	0.40	0.050	0.019	0.03	0.01	0.01	84	46	0.011	0.04	4	32
S2	K66	15X10	0.07	1.7	0.06	0.044	0.013	0.02	0.02	0.01	72	15	0.010	0.01	2	10
S1	RC1-13	10X5	0.08	0.9	0.0	0.024	0.016	0.0	0.0	0.0	90	27	0.012	0.04	3	14

*ppm

3.2.1.2. As-received micrographs

A set of five grades of microalloyed steel was investigated during this work. Metallographic preparation was carried out on the as-received specimens for microstructure examination. They were cut, mounted, ground and polished. They were then etched with 3% Nital, and the microstructure was revealed and examined using the optical microscope with a digital camera and the Olympus Stream Essential software. After examining the microstructure, it was clear that the specimens came from different origins. The 0.044% Nb-containing specimen was lab cast and the other specimens were industrially cast. For instance the 0.1% and the 0.044% Nb

specimens were cold rolled [*Figure 15* A and C] and the 0.050% and 0.024% Nb specimens were as cast [*Figure 15* B and D].
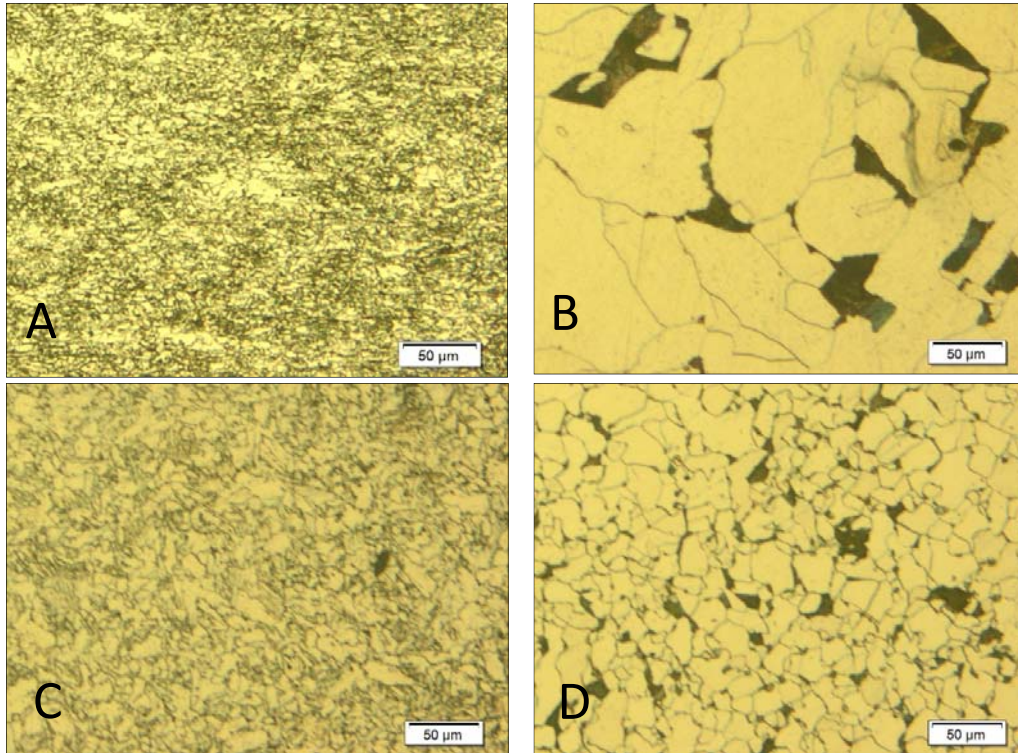
Figure 15. Micrographs of as received HSLA specimens, A (0.1% Nb), B (0.050% Nb), C (0.044% Nb) and D (0.024% Nb)

3.2.1.3. Preparation of specimen

The 0.044% Nb-containing specimen was availed in machined rods of 10 mm diameter and more or less 40 mm long while the other specimens were availed in machined rods of 5 mm diameter and 100 mm long. Having to accept the specimens' diameters "as is", the experimental materials used in this work had to be cut in cylindrical pieces of 10 mm in length and 5 mm diameter, except for the 0.044% Nb containing specimen that was cut in cylinders of 15 mm in length and 10 mm diameter. A K-type thermocouple was spot-welded on each sample for temperature measurement during the experiment.
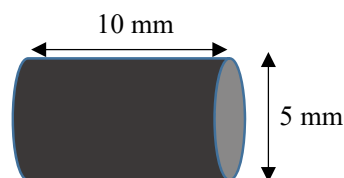
Figure 16. Compression test samples' geometry

3.2.2. Equipment

3.2.2.1. Compression test on the Gleeble

The thermo-mechanical simulator, Gleeble 1500D^{TM}, was used for hot-compression testing of the specimens. The tests were run under a neutral atmosphere (Argon gas) to avoid oxidation.

Figure 17. The Gleeble 1500D^{TM} testing machine

Figure 18. Gleeble 1500D test chamber

Figure 19. A specimen connected to a K-type thermocouple ready for a compression test in the Gleeble 1500D^{TM} test chamber

3.2.2.2. Heat treatment in the Bähr dilatometer

The cooling in the Bähr dilatometer can reach sufficiently high rates to freeze the microstructure for observation through an optical microscope. The test is run under vacuum to avoid oxidation. This high cooling rate allowed the observation and measurement of the austenite grain size.

Control and programming unit

Test chamber

Figure 20. Bähr dilatometer DL805^{TM} testing machine

Coil for sample's induction heating
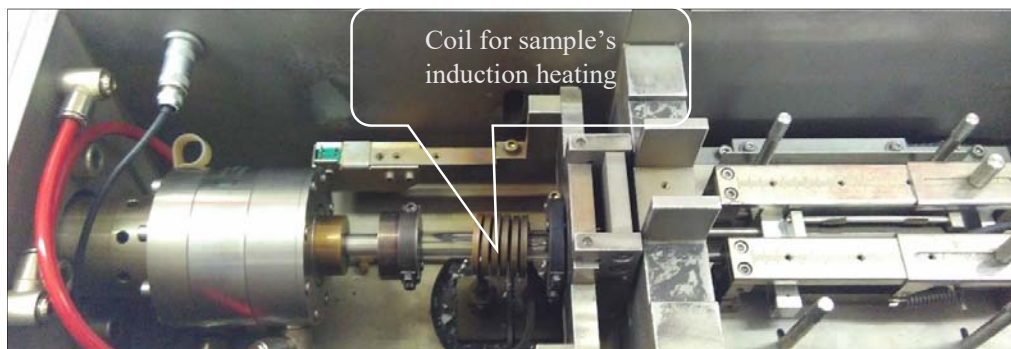
Figure 21. Bahr dilatometer DL805 test chamber

3.2.2.3. Heat treatment in the tube furnace

The as-quenched samples were heat-treated to reveal the rapidly queenched austenite microstructure [51] [52] and were thereafter tempered for 24 hours at 500 °C in a tube furnace (Figure 22). This heat treatment was done under a neutral atmosphere (argon) to avoid the sample's oxidation.

Figure 22. Tube furnace used for the tempering of as-quenched samples.

3.2.2.4. *Microstructure observation by the optical microscope*

The microstructure was observed using an optical microscope. A camera for taking images (micrographs) and a computer (using the Stream Essentials® software) for the micrograph's treatment, were used to optimise the micrographs (Figure 23).
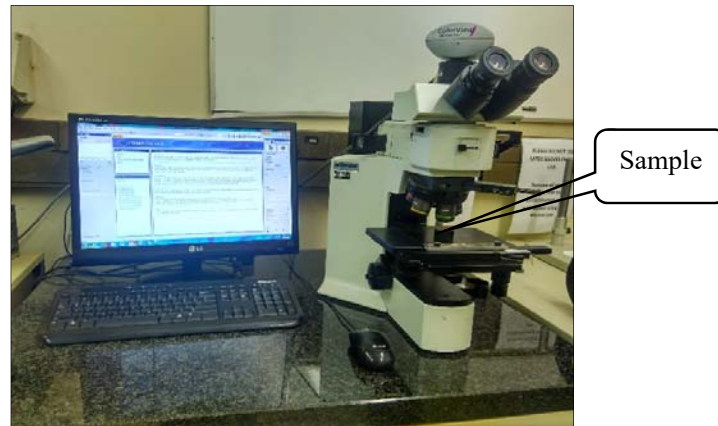
Figure 23. The optical microscope

3.3. Parameters

In previous work [6] [35], empirical equations were used to predict the critical strain for the initiation of dynamic recrystallization in a steel during hot deformation. These equations are functions of the chemical composition, the austenite grain size, the deformation temperature, and the strain rate.

$$Nb_{eff} = Nb - \frac{Mn}{120} + \frac{Si}{94} \qquad (32)$$

31

$$\varepsilon_c = \left\{0.8 - 10.8[Nb_{eff}] + 64.4\left[Nb_{eff}\right]^2\right\}\left(\frac{1 + 20Nb_{eff}}{6360}\right)D_0{}^{0.5}Z^{0.17} \qquad (33)$$

$$\varepsilon_c = (0.8 - 13Nb_{eff} + 112Nb_{eff}^2)\left\{\frac{1 + 20Nb_{eff}}{1.78}\right\} * 2.8 * 10^{-4}$$
$$* D_0^{0.5}\left\{\dot{\varepsilon} * \exp\left(\frac{375000}{RT}\right)\right\}^{0.17} \qquad (34)$$

In this work, the following parameters were studied:

- Chemical composition: The Nb content of which the influence is studied was significantly varied. The aim was to keep other alloying element contents as constant as possible but it was not easy because the samples were accepted "as is" from industry.

- Austenite grain size: In this work, the grain size was varied by soaking the samples at different austenitization temperatures with a higher soaking temperature leading to a larger initial grain (D_o).

- Deformation temperature: According to the rolling schedule provided, roughing in the industry is more or less performed by multi-passes in the temperature range from 1150 down to 1050 ºC. For the compression tests in this work, three temperatures in this range and a fourth one below the lower limit of the same range (1150, 1100, 1050, 1000 ºC) were used.

- Inter-pass time: The inter-pass time is the length of time that the material being deformed takes from one rolling pass to the next. In this work where double-hit compression experiments were performed, the inter-pass time was simulated by the time between the two consecutive compression hits. When the inter-pass time is long, the dislocation density decreases due to recovery and recrystallization and the strain accumulation will not take place. It has been shown in previous work [53] [54] that deformed microalloyed steel held at the deformation temperature (1100 ºC) becomes fully recrystallized (static recrystallization) in about 10 s. This motivated the use of inter-pass time values lower than 10 s in this study.

- Strain rate: the different rates of deformation used were 0.5, 1, 3 and 8 s^{-1}

3.4. Experiments

3.4.1. Determination of the austenite grain size

3.4.1.1. Grain boundaries

In the method which was used, the specimen was heated up to the austenitising temperature (T_A) in 15 minutes (≈1.4 ˚C/s), and soaked for 10 minutes. It was then cooled to the deformation temperature (T_{def}), and held for 10 s. This thermal cycle was applied in order to bring all of the specimens to the same condition as those before the compression test. Thereafter, the specimen was fast-quenched (600 ˚C/s) to room temperature in the Bähr dilatometer. To reveal the prior austenite microstructure, the as-quenched specimens were cut and tempered at 500 ˚C in a tube furnace for 24 hours in the presence of argon to avoid oxidation. The P and S [52] segregated to the grain boundaries and this allowed a better reaction of the prior austenitic grain boundaries with the etchant. The etchant used in this method was a mixture of 4 g of sodium dodecylbenzene sulfonic acid, 100 mL of saturated aqueous picric acid, and 100 mL of deionized water with some drops of Triton X-100 surface active reagent. An immersion of 2 to 3 minutes in the etchant heated to 80 ºC revealed the prior austenite grain boundaries.

The thermal cycle in the Bähr dilatometer of the samples for prior austenite grain size determination was as follows:
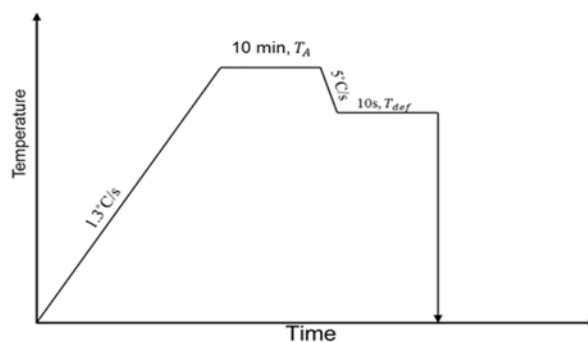
Figure 24. Thermal cycle for the austenite grain size before the compression test.

3.4.1.2. Grain size measurement

The prior austenite grain size was measured by the mean linear intercept method using the ImageJ software. A set of vertical and horizontal lines crosses the prior austenite grain boundaries on the image (Figure 25). The length of a line divided by the number of crossed

boundaries gives a measure of the intercept grain size. This estimation is done all over the micrograph area with all the lines and the final value to be considered is the average.

$$D_{gs} = \frac{\sum_i^n D_i}{n} \tag{35}$$

where, D_{gs} is the average intercept grain size, D_i is the measured grain size along the line i and n the total number of lines.
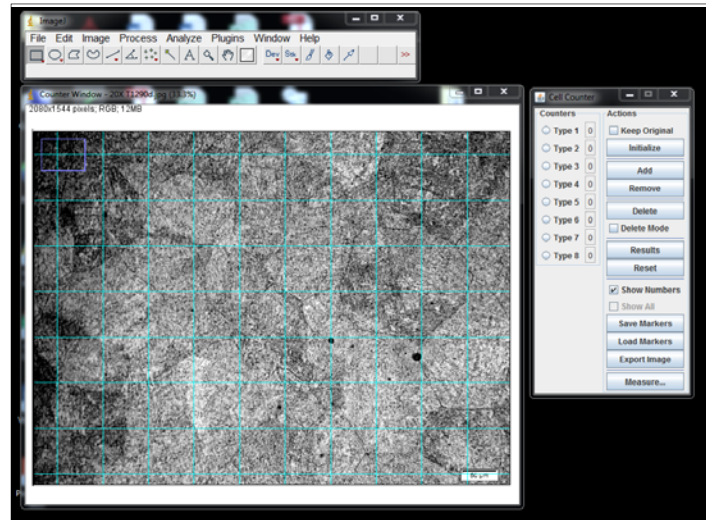
Figure 25. ImageJ software interface during grain size measurement

3.4.2. Hot-compression tests

3.4.2.1.   Gleeble

Double-hit compression tests (Figure 26) were carried out on the samples at different temperatures (1150, 1100, 1050, 1000 °C) and different strain rates (0.5, 1, and 3s^{-1}). The strain of the first pass was 0.143 and that of the second 0.7 for a total strain in the order of 0.85. The inter-pass times were also varied (0 s for single pass, 0.5, 3, and 8 s). The double-hit testing was chosen because it allowed the study of the influence of the retained strain from the first pass on the properties of the steel during the second pass. The flow stress (of the second pass) was converted to the Von Mises flow stress to obtain the Von Mises true stress-true-strain curves. A different austenite grain size was obtained by applying two different soaking (austenitising) temperatures (1200 and 1290 °C).
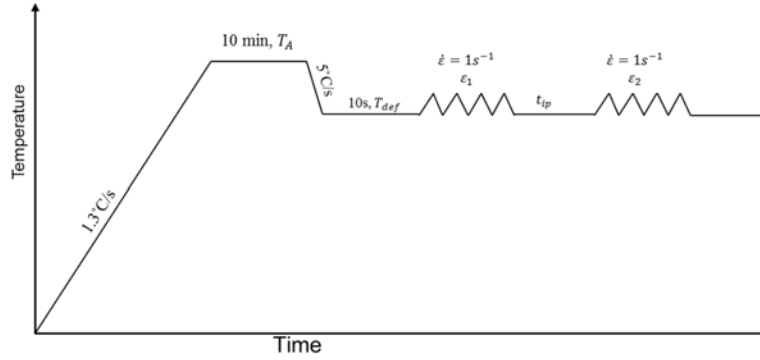
Figure 26. Double-hit compression thermomechanical cycle

3.5.   Data treatment

3.5.1. True Von Mises flow stress and true Von Mises strain

The flow curves that were experimentally obtained were plotted by converting the force-deisplacement data from the Gleeble to the Von Mises true stress σ and true strain ε. The equations [27] used for this purpose took into account the friction at the contact between the specimen and the tantalum-foil on the anvils.

$$\sigma = \frac{0.0625 P_x \mu^2 h_x^{-2}}{e^{\mu\sqrt{(d_i^2 h_i/h_x)/h_x}} - \mu\sqrt{(d_i^2 h_i/h_x)}/h_x - 1} \tag{36}$$

$$\varepsilon = \frac{2}{\sqrt{3}} ln\left(\frac{h_x}{h_i}\right) \tag{37}$$

Where, P_x is the force, h_x the stroke, h_i the initial height, d_i the initial diameter, μ the friction coefficient for steel and tantalum of which the value was 0.2

3.5.2. Finding the critical strain and stress values

A graphic method was used to find the critical strain and stress values [55]. From the plot of the work-hardening rate $\theta = d\sigma/d\varepsilon$ against the Von Mises true stress, the critical stress for the initiation of the dynamic recrystallization σ_c was determined as the inflection point, the peak stress σ_p by the first intersection of the curve with the stress axis and the steady state σ_{ss} stress by the second intersection with the stress axis (Figure 27). The critical strain ε_c for the start of DRX was determined by the inflection point on the plot of $ln\,\theta$ against the true strain (Figure 28).
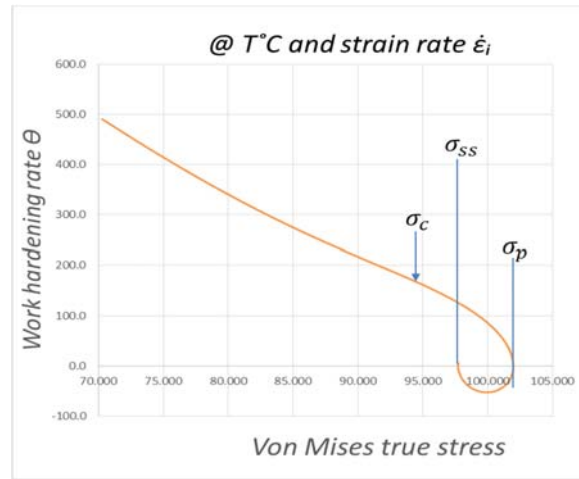
Figure 27. Graphic method for finding the critical stress values
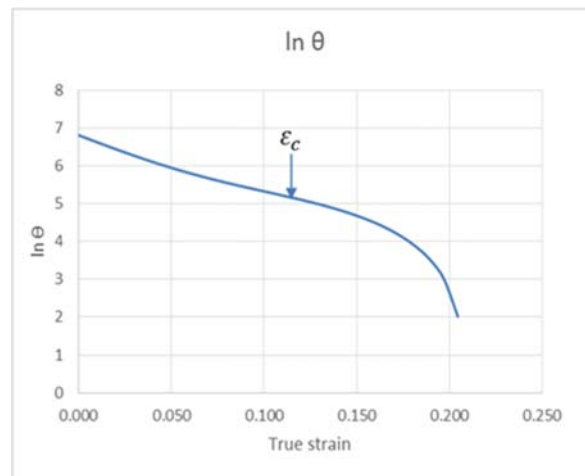
Figure 28. Graphic method for finding the critical strain for the onset of DRX

The values that were determined by these graphic methods were used for further calculations.

3.5.3. Mean flow stress (MFS)

The mean flow stress $\bar{\sigma}$ is by definition the area below the stress-strain curve normalized by the considered strain (from the initial to the final strain) [35] [56]. It describes the material's resistance to deformation [57].

$$MFS = \bar{\sigma} = \frac{1}{\varepsilon_f - \varepsilon_i} \int_{\varepsilon_i}^{\varepsilon_f} \sigma \, d\varepsilon \tag{38}$$

where, ε_i and ε_f are respectively the initial and the final true strains and σ the Von Mises true stress.

In this work, the value of the MFS was calculated by using the following equation [57]:

$$MFS = \frac{1}{\varepsilon_f - \varepsilon_i} \sum_{\varepsilon_i}^{\varepsilon_f} \sigma_{avg} \Delta\varepsilon \tag{39}$$

$$MFS = \frac{1}{\varepsilon_f - \varepsilon_i} \left[\frac{(\sigma_i + \sigma_{i+1})}{2}(\varepsilon_{i+1} - \varepsilon_i) + \frac{(\sigma_{i+1} + \sigma_{i+2})}{2}(\varepsilon_{i+2} - \varepsilon_{i+1}) \right. $$
$$\left. + \cdots + \frac{(\sigma_{f-1} + \sigma_f)}{2}(\varepsilon_f - \varepsilon_{f-1}) \right] \tag{40}$$

3.5.4. Non-recrystallization temperature

All the experiments were intended to be run at temperatures above the non-recrystallization temperature which was calculated using the Fletcher equation [17] that takes into account the strain.

$$T_{nr} = 203 - 310C - 149\sqrt{V} + 657\sqrt{Nb} + 683e^{-0.36\varepsilon} \tag{41}$$

where T_{nr} is the non-recrystallization temperature in degrees Celcius, C the carbon content, V the vanadium content, Nb the niobium content and ε the strain to which the metal was deformed.

3.5.5. Equations for hot-working constants

The literature [55] [57] provides mathematical relationships between the hot-working constants and the experimental data. The relationship between the strain rate $\dot{\varepsilon}$, the flow stress σ and the deformation temperature T is given by

$$\dot{\varepsilon} = A_n F(\sigma) \exp\left(-\frac{Q_{hw}}{RT}\right) \tag{42}$$

where, A_n is a material constant, Q_{hw} the hot-working activation energy, R the gas constant (8.314 JK^{-1}mol^{-1}), $F(\sigma)$ a function of stress

$$F(\sigma) = \begin{cases} A_2 {\sigma_{ss}}^{n_1} \\ A_3 \exp(\beta \sigma_{ss}) \\ A_1 [\sinh(\alpha \sigma_{ss})]^n \end{cases} \tag{43}$$

A_1, A_2, A_3, n, n_1, α and β are material constants and $\alpha \approx \beta / n_1$

The Zener-Hollomon parameter is:

$$Z = \dot{\varepsilon} \exp\left(\frac{Q_{hw}}{RT}\right) = A_n F(\sigma) \tag{44}$$

These equations were used to find the hot-working constants.

3.5.6. Plots and calculation to determine hot-working constants

The experimental data obtained from the isothermal single-hot-compression tests of specimens were used to plot several curves to determine hot-working constants β, n_1, α, n and Q_{hw}.

- By using the experimental data from the Gleeble 1500D®, several Von Mises true-stress-true strain ($\sigma - \varepsilon$) curves were plotted at different temperatures T and strain rates $\dot{\varepsilon}$.
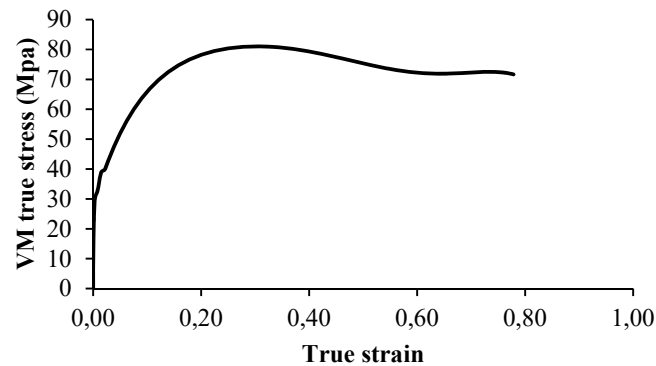
Figure 29. Example of a Von Mises true stress-true strain curve

- Referring to the equations (43) and (44), the Zener-Hollomon equation can be written as follows:

$$Z = \dot{\varepsilon} \exp\left(\frac{Q_{hw}}{RT}\right) = A_2 {\sigma_{ss}}^{n_1} \tag{45}$$

By introducing the natural logarithm function in this equation, the following expression is derived:

$$\ln \dot{\varepsilon} + \frac{Q_{hw}}{RT} = \ln A_2 + n_1 \ln \sigma_{ss}$$

(46)

The partial differentiation of this equation at a constant temperature yields the n_1 value.

$$n_1 = \left[\frac{\partial \ln \dot{\varepsilon}}{\partial \ln \sigma_{ss}} \right]_T$$

(47)

This can be seen from the following type of plot of which the slope is n_1
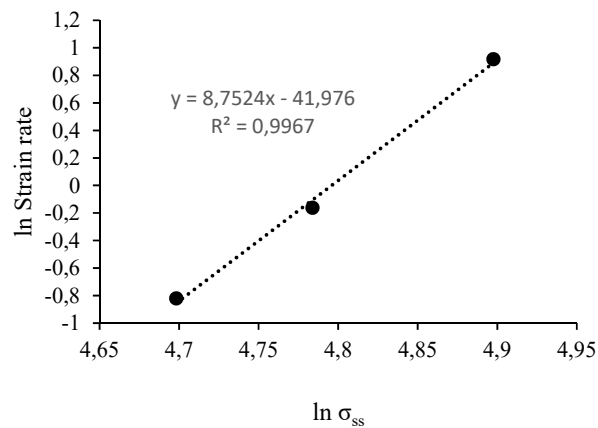
Figure 30. Example of the plot of ln strain rate versus ln steady state stress of 0.1% Nb steel at 1000°C

- Another way the Zener-Hollomon equation can be written is

$$Z = \dot{\varepsilon} \exp\left(\frac{Q_{hw}}{RT}\right) = A_3 \exp(\beta \sigma_{ss})$$

(48)

By introducing the natural logarithm function in this equation, the following expression is obtained:

$$\ln \dot{\varepsilon} + \frac{Q_{hw}}{RT} = \ln A_3 + \beta \sigma_{ss}$$

(49)

The partial differentiation of this equation at a constant temperature yields the β value,

$$\beta = \left[\frac{\partial \ln \dot{\varepsilon}}{\partial \sigma_{ss}}\right]_T \tag{50}$$

which is obtained from a plot of $\ln \dot{\varepsilon} \ vs \ \sigma_{ss}$ of which the slope will be β
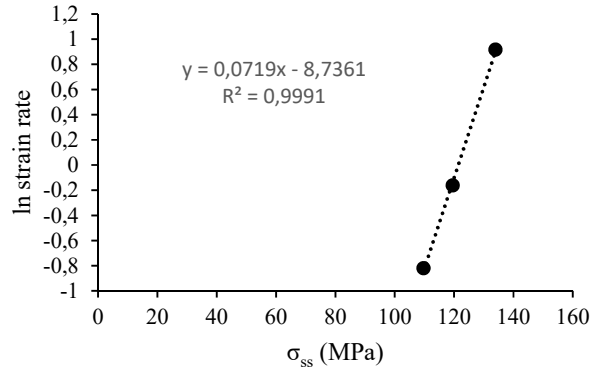
Figure 31. Example of the plot of the ln strain rate versus ln steady state stress of 0.1% Nb steel at 1000°C

- When β and n_1 are known, the value of α can be calculated:

$$\alpha = \beta/n_1 \tag{51}$$

- The third way the Zener-Hollomon equation can be written is:

$$Z = \dot{\varepsilon} \exp\left(\frac{Q_{hw}}{RT}\right) = A_1[\sinh(\alpha\sigma_{ss})]^n \tag{52}$$

When the natural logarithmic function in this equation is introduced, the following expression is derived:

$$\ln \dot{\varepsilon} + \frac{Q_{hw}}{RT} = \ln A_1 + n \ln[\sinh(\alpha\sigma_{ss})] \tag{53}$$

The partial differentiation of this equation at a constant temperature and constant strain rate yields $\left\{Q_{hw}/_{nR}\right\}$ and the n values respectively.

$$n = \left[\frac{\partial \ln \dot{\varepsilon}}{\partial \ln[\sinh(\alpha\sigma_{ss})]}\right]_T \tag{54}$$

40

$$\frac{Q_{hw}}{nR} = \left[\frac{\partial \ln[\sinh(\alpha\sigma_{ss})]}{\partial(1/T)}\right]_{\dot{\varepsilon}}$$

(55)

These can be respectively observed from a plot of $\ln\dot{\varepsilon}$ vs $\ln[\sinh(\alpha\sigma)]$ of which the slope is n and $\ln\{\sinh(\alpha\sigma_{ss})\}$ vs T^{-1} of which the slope is $\frac{Q_{hw}}{nR}$
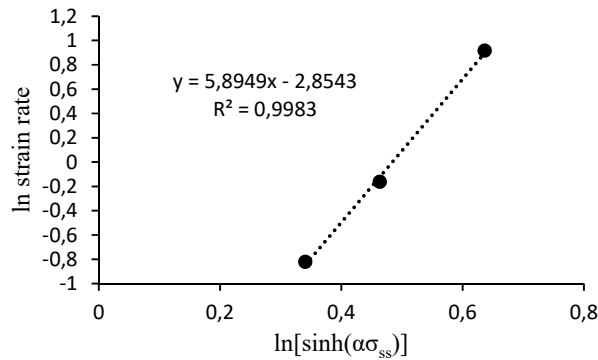
Figure 32. Example of the plot of ln strain rate versus ln sinh steady state stressof 0.1% Nb steel at 1000°C
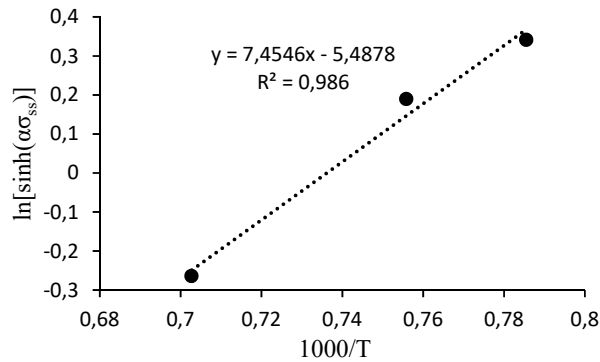
Figure 33. Example of a plot of ln sinh of steady state stress versus the inverse of temperature of 0.1% Nb steel at 0.5s^{-1}

The hot-working activation energy Q_{hw} was calculated knowing the R and n values.

3.5.7. Plot and calculations for the Z and D$_o$ exponents

In the literature [6] [35] [56] [57], the model of the critical strain ε_c for the initiation of the dynamic recrystallization is as follows:

41

$$\varepsilon_c = AZ^q D_o^m \tag{56}$$

where, A is the structural factor, Z the Zener-Hollomon parameter, D_o the initial average size of austenite grains, and q and m are dimensionless material constants.

This equation can be rewritten as follows:

$$\ln \varepsilon_c = \ln A + q \ \ln Z + m \ln D_o \tag{57}$$

$$\ln \varepsilon_c = \ln A + q \left[\ln \dot{\varepsilon} + \frac{Q_{hw}}{RT} \right] + m \ln D_o \tag{58}$$

- At a constant austenite grain size, the partial differentiation of this equation yields

$$q = \left[\frac{\partial \ln \varepsilon_c}{\partial (\ln \dot{\varepsilon} + Q_{hw}/RT)} \right]_{D_o} \tag{59}$$

A plot of $\ln \varepsilon_c$ vs $\ln Z$ produces the slope is q
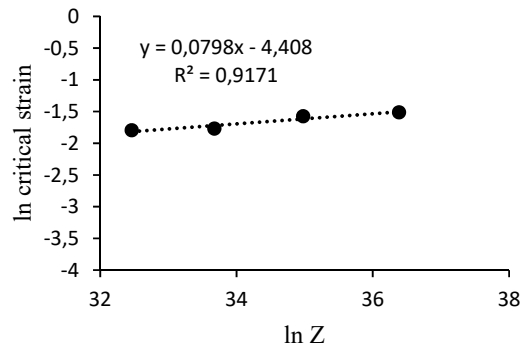
Figure 34. Influence of the Zener-Hollomon parameter on the critical strain for DRX for the 0.1%Nb steel at 0.5s⁻¹ and 1200°C(D₀=19μm).

- At a constant value of the Zener-Hollomon parameter, the partial differentiation yields

$$m = \left[\frac{\partial \ln \varepsilon_c}{\partial \ln D_0} \right]_Z \tag{60}$$

A plot of $\ln \varepsilon_c$ vs $\ln D_o$ will produce the slope m.

42
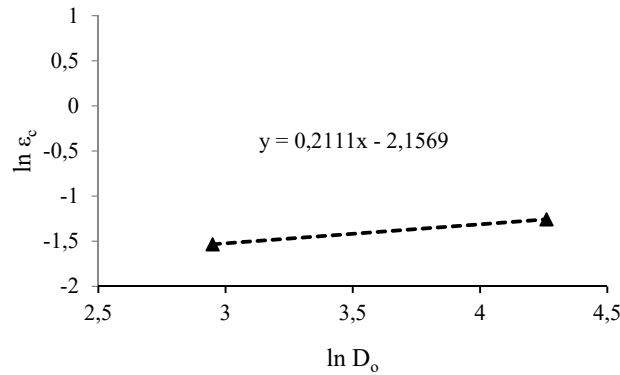
Figure 35. Influence of Do on the critical strain for the onset of DRX on 0.1%Nb steel at 1000°C

These different constants were used to develop an empirical equation that predicts the initiation of DRX as a function of the Nb% in these Nb-containing microalloyed steels.

3.5.8. Retained strain

The influence of the retained strain on the critical strain required for the onset of DRX in the following hot working pass was studied by using a double-hit deformation which allowed the use of the retained strain as an inset parameter. A partial softening occurred between two passes with the retained strain remaining that could be added to the strain applied during the second pass in order to get the total accumulated strain. The retained strain was calculated from the double-hit deformation flow curves at 0.2% of deformation. This accumulation of strain played a considerable role in the occurrence of the DRX [6].
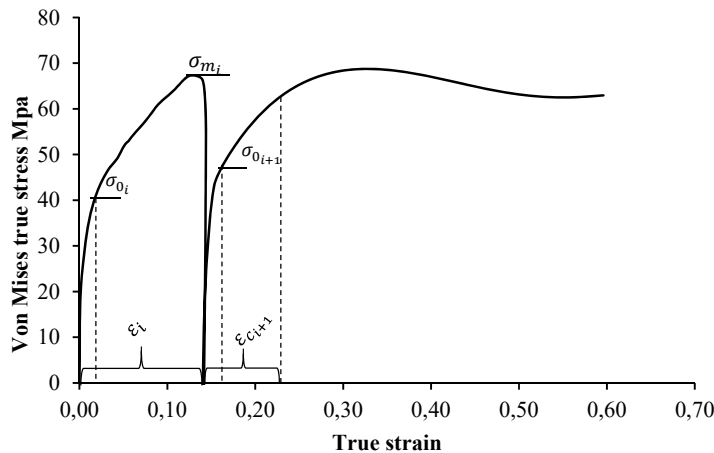
Figure 36. Schematic determination of the retained strain on a flow curve of a double-hit compression test (0.1%Nb steel at 1150°C, 0.5s^{-1} and t$_{ip}$=3s)

The retained strain was calculated as follows:

$$\varepsilon_r = (1 - X_{i+1}) * \varepsilon_i \tag{61}$$

where, X_{i+1} is the softened fraction after the initial pass and ε_i which is the initial pass strain.

The softened fraction was evaluated as follows:

$$X_{i+1} = \frac{\sigma_{m_i} - \sigma_{0_{i+1}}}{\sigma_{m_i} - \sigma_{0_i}} \tag{62}$$

where, σ_{m_i} and σ_{0_i} are respectively the maximum stress and the 0.2% the offset yield strength of the initial pass and $\sigma_{0_{i+1}}$ the 0.2% the offset yield strength of the subsequent pass.

A Johnson-Mehl-Avrami kinetic equation model [58] [59] [60] was used to develop an equation that predicted the softened fraction as a function of Nb%, inter-pass time and the deformation temperature.

$$X = 1 - e^{(Kt^n)} \tag{63}$$

where, X is the softened fraction, t the inter-pass time, and K, n are material constants.

The values of K and n were calculated for each steel as follows:

Form equation (63), we have:

$$1 - X = e^{(Kt^n)} \tag{64}$$

$$\ln(1 - X) = Kt^n \tag{65}$$

$$K = \frac{\ln(1 - X)}{t^n} \tag{66}$$

K is assumed to remain constant for two different inter-pass times, as long as the deformation temperature remains the same.

$$K = K_1 = \frac{\ln(1 - X_1)}{t_1{}^n} = K_2 = \frac{\ln(1 - X_2)}{t_2{}^n} \tag{67}$$

44

$$\left(\frac{t_1}{t_2}\right)^n = \frac{\ln(1 - X_1)}{\ln(1 - X_2)} \tag{68}$$

$$n = \frac{\ln\left[\frac{\ln(1 - X_1)}{\ln(1 - X_2)}\right]}{\ln\left(\frac{t_1}{t_2}\right)} \tag{69}$$

After the material constants K and n had been obtained for the different steels, the expression (Kt^n) was reformulated as a function of inter-pass time, niobium content in % and deformation temperature in K $(t_{ip}, [Nb], T)$ for modelling purposes.

From the equation (63):

$$X = 1 - e^{Kt_{ip}^n} = 1 - e^{f(t_{ip},[Nb],T)} \tag{70}$$

and the retained strain was then given by:

$$\varepsilon_r = \varepsilon_i * \left[1 - \left\{1 - e^{f(t_{ip},[Nb],T)}\right\}\right] \tag{71}$$

or,

$$\varepsilon_r = \varepsilon_i * e^{f(t_{ip},[Nb],T)} \tag{72}$$

The modelling of this function was as follows:

$$f\left(t_{ip}, \ [Nb], \ T\right) = a \ t_{ip} + b \tag{73}$$

where a and b are sub-functions of the [Nb] content,

$$a = f([Nb], \ T) = c \ [Nb] + d$$
$$b = f([Nb], \ T) = r \ [Nb] + s \tag{74}$$

Where c, d, r and s are functions of the deformation temperature in K,

$$c, d, r, s = f(T) \tag{75}$$

3.6. Development of the model

The equation that was developed for the critical strain for initiation of DRX and that of the retained strain, were combined to produce a constitutive model. This combination predicts the critical strain for the onset of dynamic recrystallization, taking into account the retained strain from a previous deformation. It includes in fact two functions: the critical strain for the onset of DRX in a single pass (ε_c) and the retained strain from the previous pass (ε_{r_i}). This empirical model is valid only during roughing above T_{NR} (above 1000ºC).

$$\varepsilon_{c_{i+1}} = \aleph\left(\varepsilon_c, \varepsilon_{r_i}\right) \qquad (76)$$

4. RESULTS

4.1. Introduction

This section sets out the key experimental results.

4.2. Thermo-calc® prediction

The Thermo-calc® software was used to predict the expected different phases that could precipitate in the steel at the deformation temperature during the test. NbC (with some Ti and N), TiN (with some Nb and C) and MnS (with some Ca) were the significant phases that could precipitate according to the software prediction. Other minor precipitates such AlN and BN were also noticed through the prediction. More attention was paid to NbC, because its amount varied from one specimen to another due to the variation in the Nb content. The software also allowed the prediction of the optimal solution temperature for these precipitates.
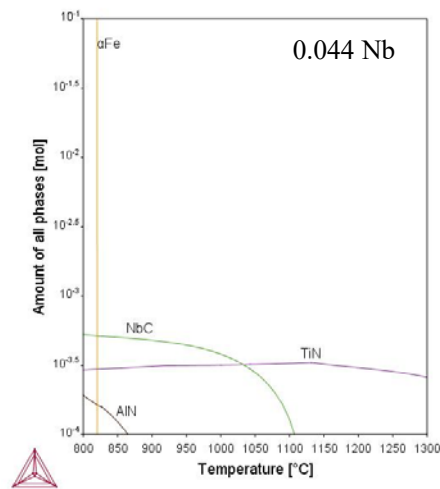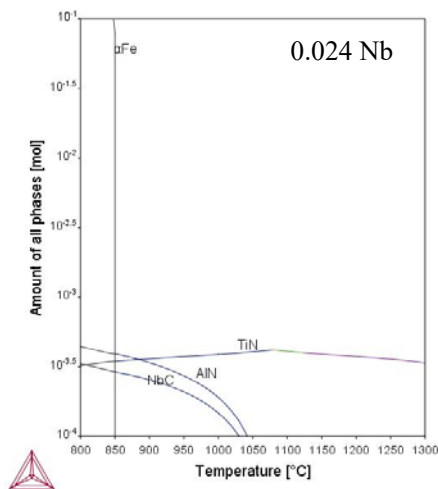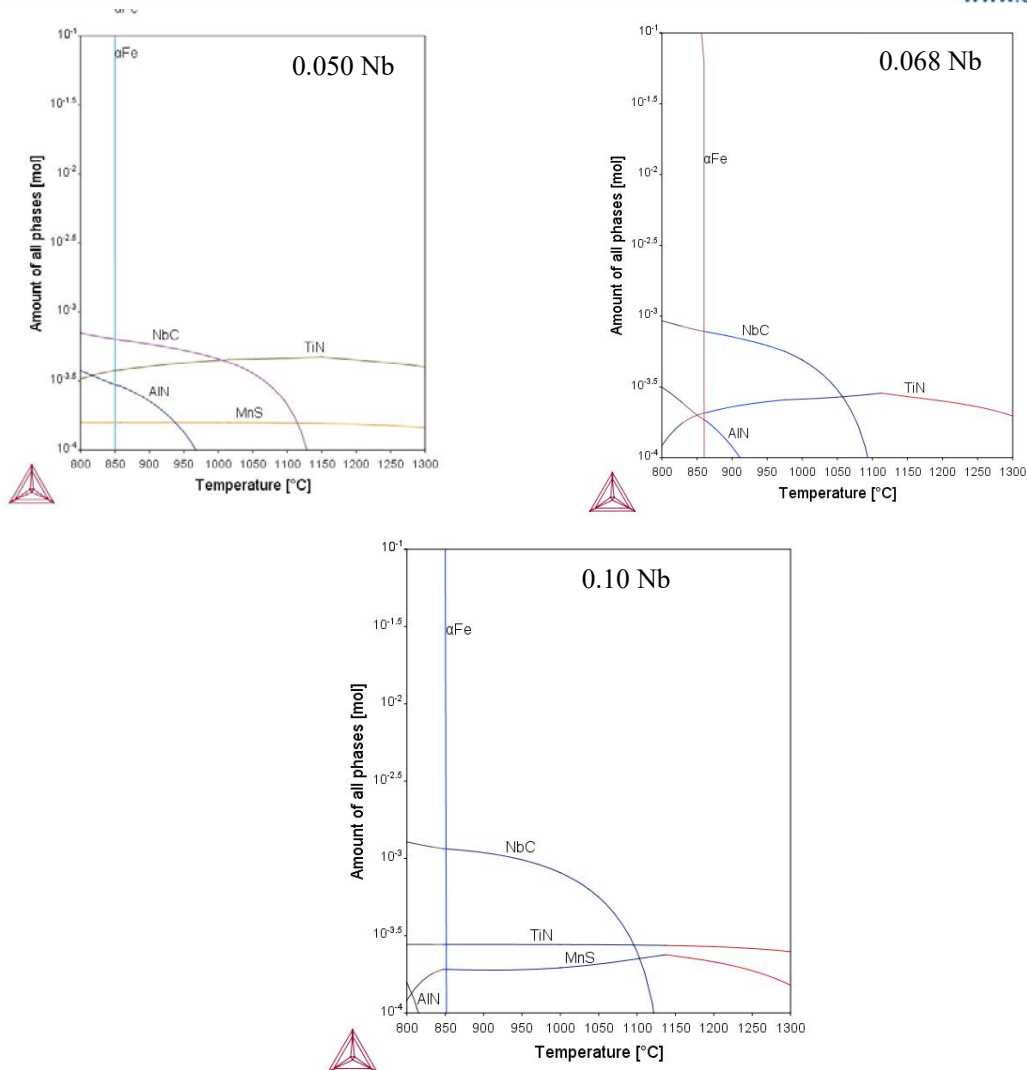
Figure 37. Prediction of solution temperatures of precipitating phases through Thermo-calc® software.

According to this prediction, the NbC is completely in solution above 1150 ºC (Figure 37) and the two soaking temperatures were set at 1200 ºC and 1290 ºC, the later to introduce some austenite grain growth prior to hot working.

4.3. Mean flow stress (MFS)

4.3.1. Background

The determination of the MFS allowed a better understanding of the behaviour of the steel as it represented the overall resistance to hot deformation in each steel [57].

4.3.2. Effect of Nb on the Mean Flow Stress

It was observed that the MFS increased slightly with the addition of Nb to the steel due to carbide precipitation or atomic solute drag [45] [46]. It may be seen however in Figure 38,

that the Nb addition was no longer effective beyond 0.068%. This observation is in agreement with the effect of Nb on the hardness, where there is no longer any effect above 0.068% Nb, see *Table 4*.
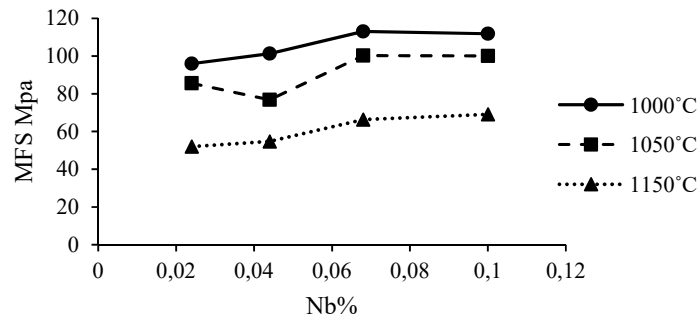
Figure 38. Effect of Nb content and deformation temperature on the mean flow stress.

When Nb is added for strengthening purposes to Nb-bearing microalloyed steels, there is no need to increase the content beyond about 0.07%. The addition of Nb is responsible of more solute drag effect and precipitation strengthening in microalloyed steels [46], and this is very clearly observed in the effect on the MFS due to more difficulty for dislocations to overcome the effect of Nb solute drag at high temperatures or precipitates at low temperatures [61] [62].

Table 2. Thermo-Calc® prediction of Nb precipitation depending on temperature

	% Nb$_{(in\ precipitates)}$ / % Nb$_{(total)}$				
T°C	S1	S2	S3	S4	S5
1000	0,0059	0,0078	0,0076	0,0067	0,0064
1050	0,0000	0,0054	0,0063	0,0037	0,0050
1100	0,0000	0,0027	0,0035	0,0000	0,0021
1150	0,0000	0,0000	0,0000	0,0000	0,0000

According to Thermo-Calc predictions, the Nb was in solution at the soaking temperature and only a small portion precipitated during the deformation tests.

4.4. Prior austenite grain size

4.4.1. Effect of soaking temperature on austenite grain size

The soaking was performed at two different temperatures to vary the austenite grain size. From room temperature, at the rate of 1.3˚C/s, the samples were heated up to 1200 and 1290˚C and soaked for 10 minutes, and then they were cooled at 5˚C/s to 1000˚C.
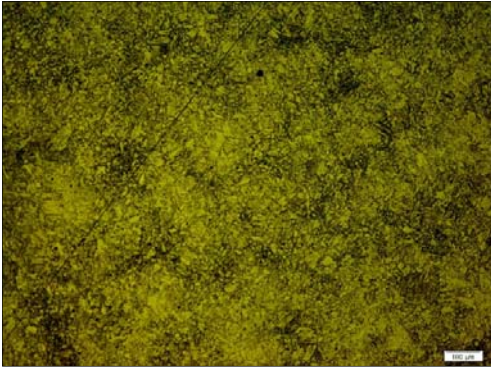
0.024 Nb soaked at 1200 ˚C
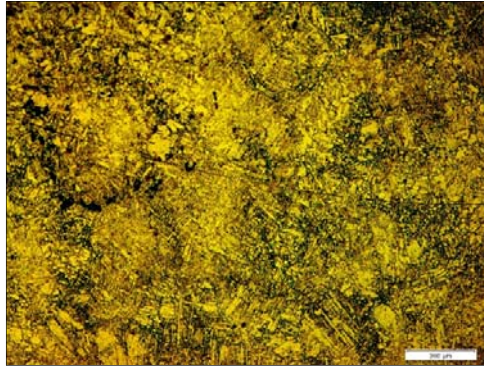
0.024 Nb soaked at 1290 ˚C
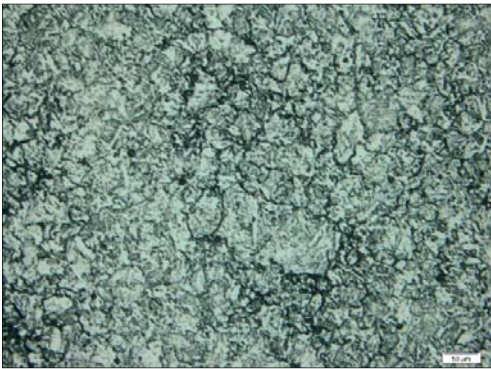
0.050 Nb soaked at 1200 ˚C
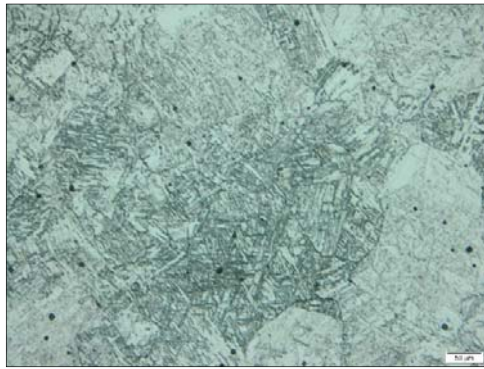
0.050 Nb soaked at 1290 ˚C
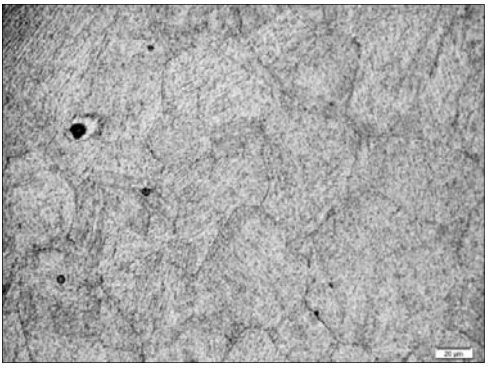
0.068 Nb soaked at 1200 ˚C
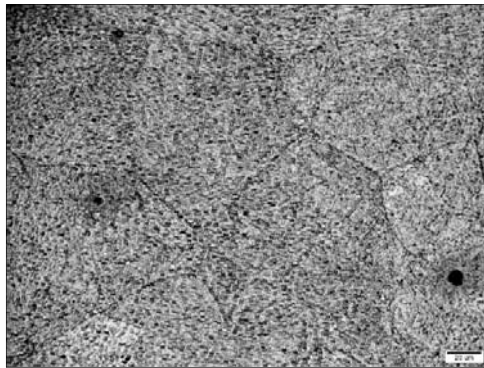
0.068 Nb soaked at 1290 ˚C
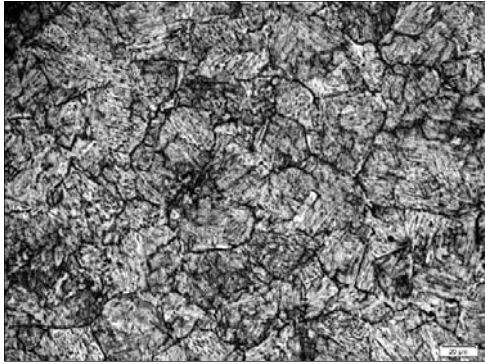
0.1 Nb soaked at 1200 ˚C
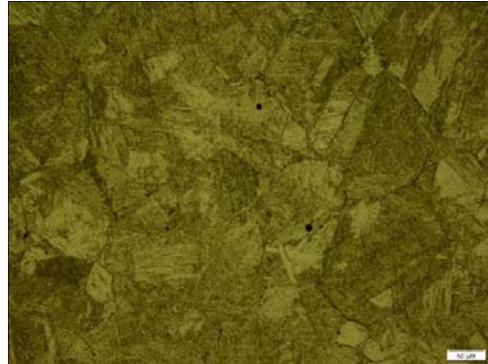
0.1 Nb soaked at 1290 ˚C

Figure 39. Micrographs of Nb steel specimens soaked for 10 minutes at 1200 ˚C (left) and 1290 ˚C (right) for a different grain size.

After holding the specimens at the reheating temperature for the same length of time, the larger grain size was observed in the samples which were soaked at higher temperature.

Table 3. Average prior austenite grain size at different austenitising temperatures.

	Average prior austenite grain size (µm)			
Steels	S1	S3	S4	S5
Nb %	0.024	0.050	0.068	0.100
$D_{0\ 1200}$	197±30	50±8	38±10	19±3
$D_{0\ 1290}$	221±73	96±17	74±15	71±15

4.4.2. Effect of Nb content on the austenite grain size

It was observed that as the Nb content was increased, the austenite grain size decreased to a minimum with only minimal further decreases.
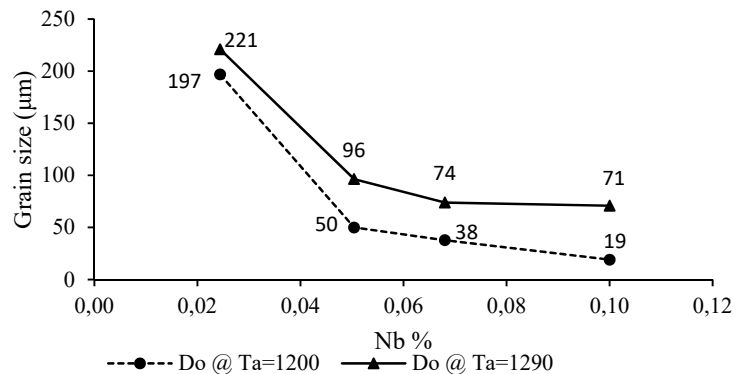
Figure 40. Effect of Nb content on the austenite grain size at different soaking temperatures.

4.5. Hardness

The Brinell hardness (HB) was measured on a set of samples after reheating at 1200 ºC, a double-hit compression test at 1050ºC with 0.5 s inter-pass time and slow cooling under argon atmosphere. It allowed a better understanding of the effect of Nb on the mechanical properties after hot working.

Table 4. Effect of Nb content on the hardness after double hit compression at 1050°C with t_{ip}=0.5s

ID	S1	S2	S3	S4	S5
Nb%	0.024	0.044	0.050	0.068	0.100
HB	63	83	85	91	90

After the experimental compression test, it was observed that the hardness increased with the addition of niobium but became largely ineffective from about 0.068% (Figure 41).
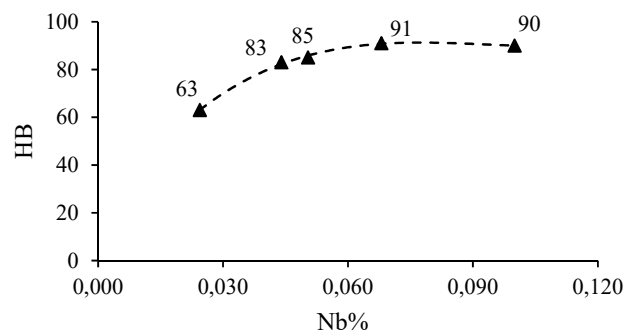
Figure 41. Influence of the Nb content on the Brinell hardness (HB) after double hit compression at 1050°C

4.6. The exponent (m) of the initial austenite grain size on the critical strain ε_c for DRX

4.6.1. Background

The austenite grain size has a measurable effect on the critical strain for the onset of DRX to an extent that is determined by the exponent (*m*) in the critical strain in Equation (56). This exponent was determined as the slope of the plot of the natural logarithm of the critical strain against the natural logarithm of the prior austenite grain size as had been shown in Figure 35.

4.6.2. Influence of Nb on the exponent of the austenite grain size

It was noticed that this exponent's value was influenced by the Nb content in the steel. A linear relationship described the reduction of this value with addition of Nb; see Table 5 and Equation (77).

Table 5. Effect of Nb content on the austenite grain size exponent m on th onset of DRX

	S1	S3	S4	S5
Nb%	0.024	0.050	0.068	0.10
m experimental	0.389	0.332	0.283	0.214
m calculated	0.387	0.327	0.286	0.212

The soaking of specimens after the reheating was performed at two different temperatures (1200 and 1290°C). There were then two different austenite grain sizes per chemical composition. Consequently, the straight line of which the slope represents the value of m was drawn from only two points. With more experiments, the addition of a third point would have been better for greater accuracy of the value of m.

$$m = -2.3132[Nb] + 0.4437 \tag{77}$$

where, *m* the exponent of the austenite grain size is dimensionless and [Nb] is the mass percentage of niobium in the steel. This equation was used to calculate the value of the austenite grain size exponent as a function of the Nb% and showed a good fit with the experimental data (Figure 42).
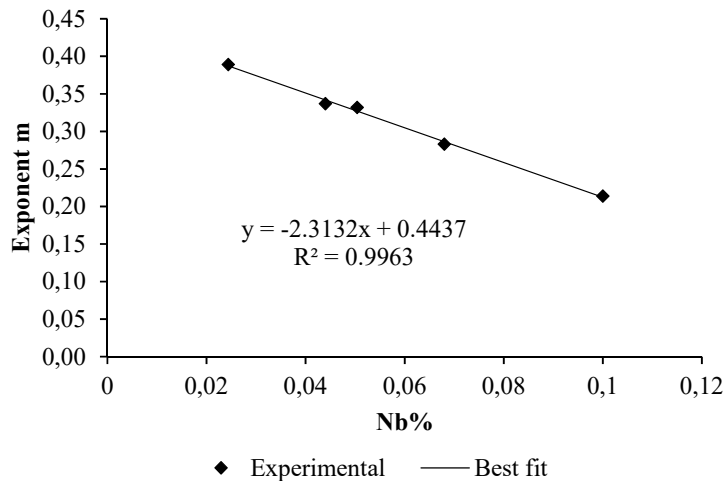
Figure 42. Influence of Nb content on the value of the austenite grain size exponent m for the onset of DRX.

53

4.7. Zener-Hollomon parameter

4.7.1. Background

The Zener-Hollomon parameter (Z) or the temperature-compensated strain rate, was calculated for different temperatures and strain rates, but the hot-working activation energy first had to be determined (Equation 1).

4.7.2. Effect of Nb on hot-working activation energy

The values of the hot-working activation energy (Q_{hw}) were determined for all the specimens with different Nb contents by using the experimental data from the Gleeble 1500D® during the compression tests.

A constitutive equation to calculate the hot-working activation energy (Figure 43) as a function of Nb weight percentage was developed as follows:

$$Q_{hw}(kJ/mol) = -26856[Nb]^2 + 4948.9\,[Nb] + 170.32 \tag{78}$$

where, Q_{hw} is the hot-working activation energy in *kJ/mol* and [Nb] the mass percentage of niobium.
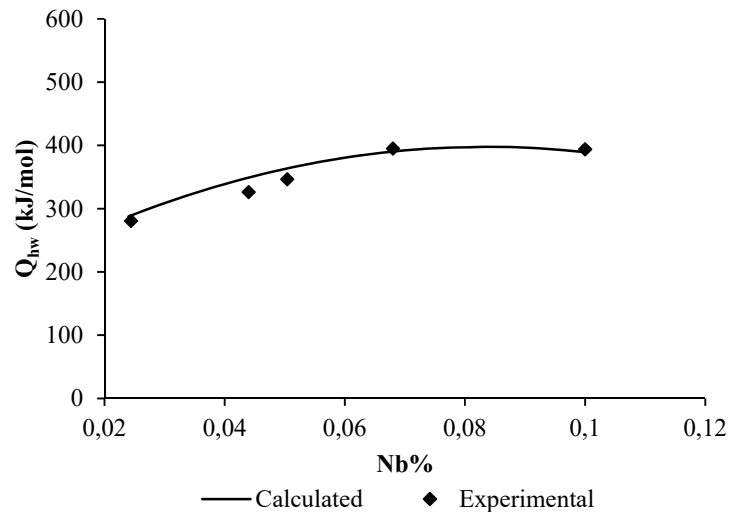
Figure 43. Effect of Nb content on the hot-working activation energy

The Zener-Hollomon parameter can now be determined for a known temperature and strain rate by using the following equation:

$$Z = \dot{\varepsilon}\exp\left(\frac{Q_{hw}}{RT}\right) \tag{79}$$

4.8. The exponent q of the Zener-Hollomon parameter

4.8.1. Background

The critical strain for DRX is dependent on the deformation conditions that are expressed by the Zener-Hollomon parameter Z to an extent that is determined by the exponent (q) in the Equation (56). This exponent was determined from the slope of the plot of the natural logarithm of the critical strain ε_c against the natural logarithm of the Zener-Hollomon parameter Z.

4.8.2. Influence of Nb on the exponent q of Z

The Nb content had an effect on the value of the exponent q of the Zener-Hollomon parameter. The exponent was constant ($q \approx 0.142$) from 0.024%Nb to 0.050%Nb and went down ($q \approx 0.081$) and remained again constant from 0.068%Nb to 0.10%Nb. It appeared two regimes were present.

Table 6. Effect of Nb content on the Zener-Hollomon exponent q

	S1	S2	S3	S4	S5
Nb%	0.0244	0.044	0.0504	0.068	0.1
q_{1200}	0.149	0.142	0.140	0.082	0.079
q_{1290}	0.141	0.145	0.137	0.087	0.079

The soaking temperature was varied to produce different prior austenite grain sizes. Almost no influence on the exponent of the Zener-Hollomon Z was observed while the soaking temperature (austenite grain size) was being varied. The equations obtained were as follows:

$$q = \begin{cases} 0.142 \ for \ Nb < 0.068 \\ 0.081 \ for \ Nb \geq 0.068 \end{cases} \tag{80}$$

The calculated values for the two different austenitising temperatures in each case were very close. The soaking temperature has therefore no effect on the Zener-Hollomon exponent.

4.9. The structural factor

4.9.1. Background

The structural factor A is a material constant that can vary with the chemical composition. It was determined for each grade of the experimental steels by dividing the critical strain for the initiation of DRX by the product $Z^q D_o{}^m$.

4.9.2. Influence of Nb content on the structural factor A

The experimental data (Figure 44) showed how the structural factor A increased with the progressive addition of Nb content, while the *q* exponent decreased. An effect was no longer observed when the Nb content reached 0.068%, the structural factor tended to remain constant from this Nb percentage as observed from the hardness, the grain size and the hot-working activation energy. An equation predicting the value of the structural factor A as a function of Nb content was developed by using data-fitting methods.

Table 7. Effect of Nb content on the structural factor A

	S1	S2	S3	S4	S5
Nb%	0.024	0.044	0.050	0.068	0.100
A Experimental	5.72E-04	5.97E-04	6.16E-04	3.02E-03	6.63E-03
A Predicted	5.72E-04	5.82E-04	6.39E-04	3.14E-03	6.59E-03

The four-parameter logistic function was used here to obtain an equation (81) that fitted the experimental data. It was then possible to calculate the structural factor as a function of the Nb content.

$$A = \frac{0.006058}{1 + \left(\frac{[Nb]}{0.0695}\right)^{-14}} + 5.72 * 10^{-4} \tag{81}$$

where, *A* is the structural factor (without dimension) and $[Nb]$ the weight percentage of niobium in the steel.
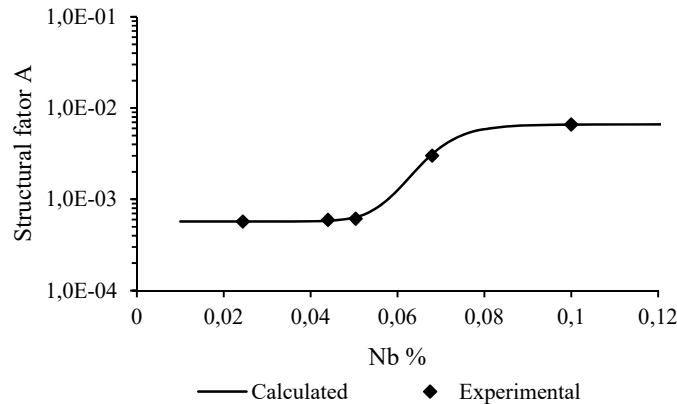
Figure 44. Effect of Nb content on the structural factor A

4.10. Dynamic recrystallization

4.10.1. Background

The critical strain for initiation of DRX for a single pass is represented by an expression as follows:

$$\varepsilon_c = A \, Z^q D_o{}^m \tag{82}$$

where, ε_c is the critical strain for DRX initiation, A, q and m are material constants, Z is the Zener-Hollomon parameter also known as the temperature-compensated strain rate parameter and D_o is the prior austenite grain size.

4.10.2. Contribution of different parameters to the critical strain for the onset of DRX

The experimental data allowed the establishment of functions of the chemical composition (Nb content) that could predict the value of material constants A, q and m from Equation (82).

Table 8. Material constants as function of Nb content

Structural factor A	$A = \dfrac{0.006058}{1 + \left(\dfrac{[Nb]}{0.0695}\right)^{-14}} + 5.72 * 10^{-4}$
Zener-Hollomon exponent q	$q = \begin{cases} 0.142 \ for \ [Nb] < 0.068 \\ 0.081 \ for \ [Nb] \geq 0.068 \end{cases}$
Austenite grain size exponent m	$m = -2.3132[Nb] + 0.4437$

These equations were combined to establish the critical strain for the onset of the dynamic recrystallization for a single pass as follows:

$$\varepsilon_c = \left[\dfrac{0.006058}{1 + \left(\dfrac{[Nb]}{0.0695}\right)^{-14}} + 5.72 * 10^{-4}\right] * Z^q * D_o{}^{(-2.3132[Nb]+0.4437)} \tag{83}$$

4.10.3. Influence of the pre-strain on the critical strain

A pre-strain ($\varepsilon_1 \cong 0.142$) was introduced (Figure 46) to the steel before the application of an inter-pass time and the second deformation. The pre-deformation amount was kept lower than that of the critical strain for a single pass so that no DRX could be initiated before the second pass. It was observed that the critical amount of strain for the DRX initiation during the

second pass deformation was noticeably lower than that during a single pass (Figure 45, Figure 46 and Figure 47) in the same conditions (temperature and strain rate). This is due to the amount of strain that remains in the steel after the first pass and the partial softening during the inter-pass time. This retained strain acts as an additional driving force for the DRX in the actual pass.
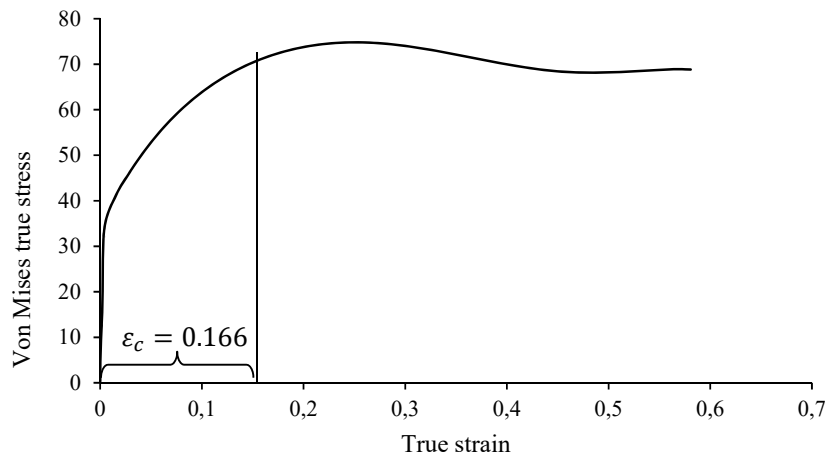
Figure 45. Flow curve of a single-pass deformation test of a 0.10 Nb% microalloyed steel at T_{def}=1150 ºC, T_a=1200 ˚C and $\dot{\varepsilon}$=0.5 s⁻¹
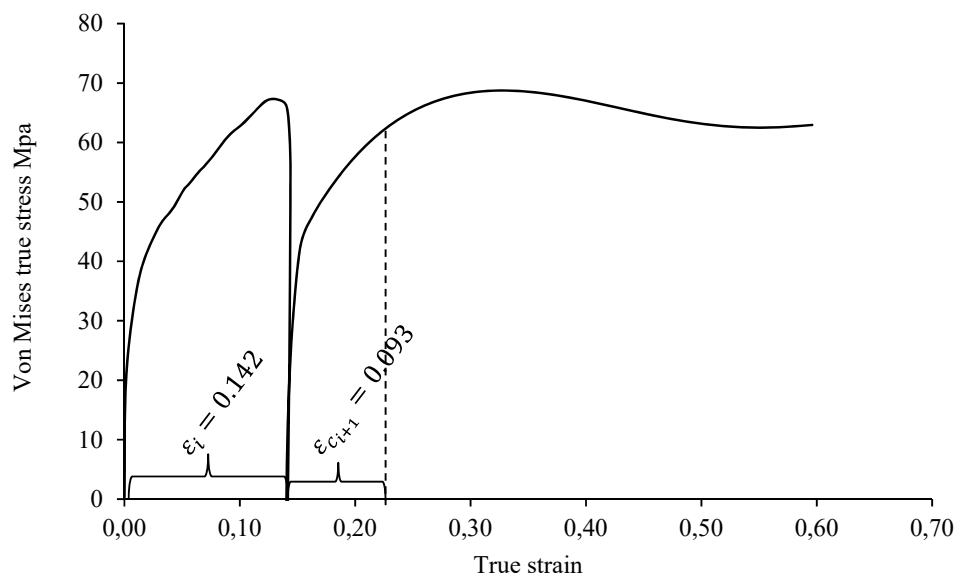
Figure 46. Flow curve of a double hit deformation test of a 0.10%Nb microalloyed steel at T_{def}=1150 ºC, T_a=1200 ºC and $\dot{\varepsilon}$=0.5 s⁻¹ with an inter-pass time of t_{ip}=0.5 s

The introduction of a pre-strain decreased the amount of deformation required for the initiation of DRX (Figure 47). This pre-deformation was more effective when the inter-pass time was shorter because the steel did not have enough time for a softening mechanism that would progressively bring back the original mechanical properties (microstructure) of the steel.
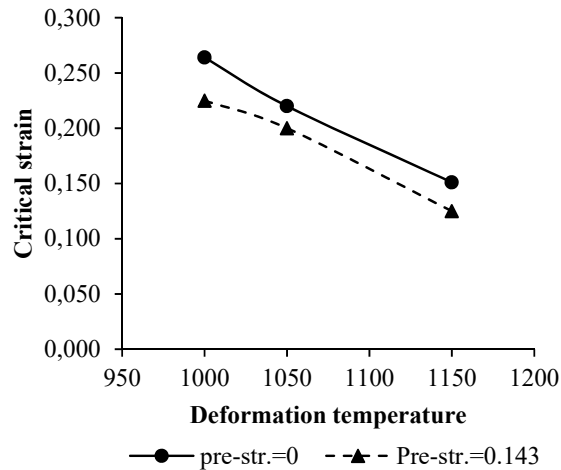
Figure 47. Effect of a pre-deformation (t_{ip}=3s) on the critical strain for DRX initiation of a 0.044 Nb% HSLA steel.

4.11. Retained strain

4.11.1. Background

The samples were strained at 0.143 during the first pass and after an inter-pass time, the retained strain was taken into account for the evaluation of the amount of strain that was necessary to initiate the dynamic recrystallization in the second-pass' deformation. When the amount of retained strain was high, the critical strain for DRX during the second pass was lower. The test was not performed on the sample with 0.068%Nb at 1100°C due to limited amount of specimens.
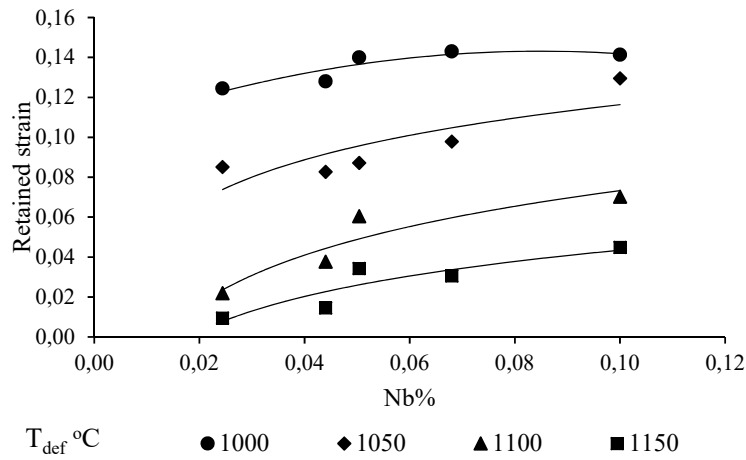
Figure 48. Effect of deformation temperature and Nb content on the retained strain after a first pass strain of 0.143 and an inter-pass time of 3 s
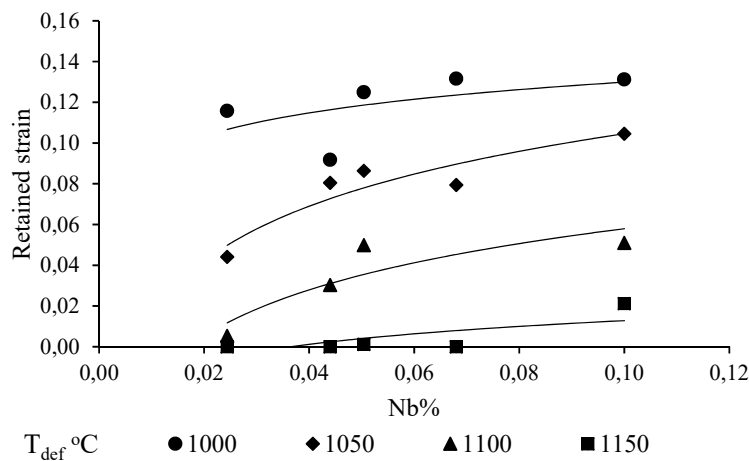
Figure 49. Effect of deformation temperature and Nb content on the retained strain after a first pass strain of 0.143 and an inter-pass time of 8 s

4.11.2. Influence of the deformation temperature on the retained strain

At higher deformation temperatures, the amount of retained strain was lower (Figure 48 and Figure 49), due to higher available driving force or thermal activation energy for the softening mechanism during the inter-pass time [63].

4.11.3. Influence of the inter-pass time on the retained strain

It was noticed that the retained strain decreased as the time became longer between the two hits. A longer time will allow more rearrangement and restoration [54].

4.11.4. Influence of Nb content on the retained strain

It was observed that there was less softening (more retained strain) in the steels containing more Nb. Niobium as an alloying element retarded the occurrence of softening mechanisms also in other studies [42] [43].

4.11.5. Contribution of different parameters to the retained strain

The retained strain was evaluated by a constitutive equation that took into account the amount of the pre-strain, the inter-pass time, the deformation temperature and the niobium content.

$$\varepsilon_r = \varepsilon_i * e^{f(t_{ip}, Nb\%, T)} \tag{84}$$

Double-hit deformation tests were conducted in the Gleeble for all specimens, varying the temperature from 1000 °C to 1150 °C, the inter-pass time from 0.5 to 8 s, and the Nb content from 0.024 to 0.1%. The strain rate was kept unchanged (0.5 s^{-1}). The amount of retained strain was calculated from the experimental data and the results were used to establish an equation that could predict the amount of retained strain after a fixed pre-deformation ($\varepsilon_1 \cong 0.142$), at a given temperature and inter-pass time.

From the experimental results (Table 12), the following constitutive equation was developed:

$$\varepsilon_r = \varepsilon_i * e^{[(0.056T-71.707)\,[Nb]-0.0068T+8.7081]t_{ip}+(-0.0391T+50.81)\,[Nb]+0.0018T-2.2703} \tag{85}$$

with the [Nb] content in mass percent, the temperature in K and the inter-pass time in seconds.

4.12.   Development of the empirical model

4.12.1. Background

The amount of strain required to initiate the dynamic recrystallization after a pre-deformation was lower than that of a single pass without any pre-strain (Table 12). This was due to the retained strain that contributed to the amount of strain that acted as an additional driving force for the DRX initiation during the second pass. The amount of retained strain was as expected a fraction of the pre-strain. The pre-deformation (pre-strain) was kept lower than the critical strain for DRX onset of a single pass. It is assumed that the retained strain was consequently lower than the critical strain of DRX initiation.

4.12.2. Model

From the combination of the two functions, an empirical equation was developed for the prediction of the critical strain for the onset of the DRX which took into account the retained strain. The overall expression was a complex function of niobium content ($Nb\%$), austenite grain size (D_o), strain rate ($\dot{\varepsilon}$) and deformation temperature (T), combined in the Zener-Hollomon parameter (Z), inter-pass time (t_{ip}), and the pre-strain of the steel (ε_i).

$$\varepsilon_{c_{i+1}} = \aleph\left(\varepsilon_c, \varepsilon_{r_i}\right) \tag{86}$$

Further observation showed that the strain needed during the second pass to initiate the DRX added to the retained strain yielded an amount of strain very close to the critical strain for DRX onset during a single-pass deformation. Hence, the amount of strain needed for DRX after introduction of a pre-strain was estimated by subtracting the retained strain from the amount of strain required for DRX during a single pass.

$$\varepsilon_{c_{i+1}} = \varepsilon_c - \varepsilon_{r_i} \tag{87}$$

where, ε_c and ε_r are respectively given in Equations (83) and (85)

5. DISCUSSION

5.1. Introduction

In this section, the key results will be interpreted and explained. This section will not only show how this work answers the problem statement but will also justify the approach and critically evaluate the study.

5.2. Double hit compression tests

For the investigation of the influence of the retained strain on the critical strain for DRX's initiation, the chosen method was the double hit compression test where the main studied parameters (Nb content, austenite grain size, deformation temperature, inter-pass time, strain rate) were consequently varied. The amount of retained strain was modified by varying the inter-pass time between the two consecutive passes. The analysis of the results was done on the flow curve of the second pass. The austenite grain size was a difficult parameter to handle right after the inter-pass time. This method did not allow a reliable measurement of austenite grain size as after the inter-pass time, as it was a mixture of deformed, recovered and possibly recrystallized grains. Finally, the considered austenite grain size D_0 was the one prior to the first pass.

5.3. Austenite grain size

The refinement of the austenite grains was due to the presence of Nb, which acted as a grain refiner by precipitate-pinning and by solute drag effect [42]. The refining role of Nb on the austenite grain size appeared to be no longer effective from 0.068% Nb upwards as above this amount, no major change was noticed. This observation is in agreement with the effect of Nb on the hardness (Figure 41) where there is also no longer an effect beyond 0.068% Nb. Below this "ceiling value" of Nb%, a higher Nb% promoted a smaller austenite grain size which transformed in finer ferrite [1] [64] that is responsible of the material strength (Hall-Petch relationship) [65] [66].

5.4. Zener-Hollomon Parameter

The temperature compensated strain rate parameter Z is dependent on the hot working activation energy (2.1.1). The experimentally obtained results of the hot working activation energy were compared to the values that were obtained using equations that Liquiang and Medina [34] [43] [67] proposed to calculate the hot-working activation energy also in Nb-containing microalloyed steels (Figure 50).

It was confirmed in this study as well as in the studies of Liquiang and Medina [34] [43] that regardless of the predicted or the experimental values, the hot-working activation energy increased as Nb was added, but remained constant at values exceeding approximately 0.07%Nb. It can be assumed that above this value, the steel became insensitive to more Nb and no further effect was observed (Figure 43). This observation was again in agreement with the effect of Nb on the austenite grain size, and the mean flow stress (no effect above 0.068%).

The equation shown on the figure: $y = -26856x^2 + 4948{,}9x + 170{,}32$
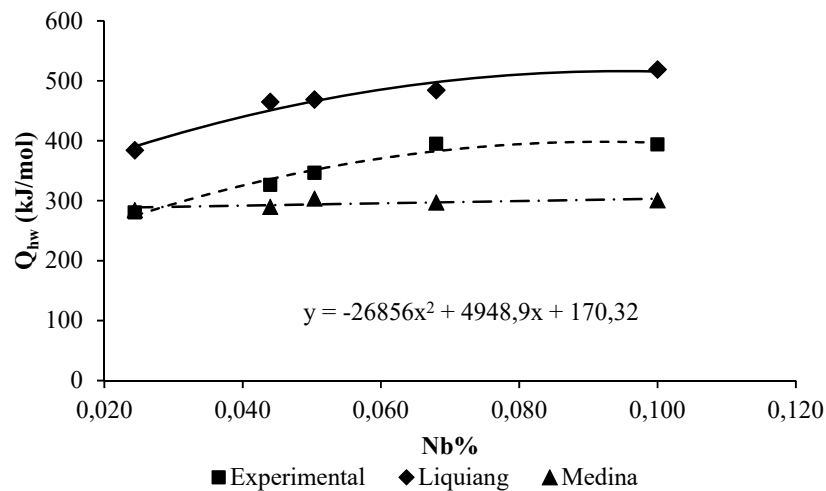
Figure 50. Influence of Nb on the hot-working activation energy in HSLA Nb containing steels.

The values obtained from Liquiang's equation were not equal to those of this work, due to the use of different steel chemistries. The strain rate during his experiments reached $5s^{-1}$ and only the titanium content was varied while other alloying elements were kept constant.

Table 9. Chemical composition of Liquiang's work samples [34]

Steel	C	Si	Mn	P	S	Nb	Ti	N
N-T0	0.11	0.17	1.23	0.006	0.005	0.038	0	0.002
N-T1	0.11	0.18	1.19	0.005	0.005	0.04	0.015	0.002
N-T2	0.12	0.23	1.22	0.005	0.005	0.043	0.027	0.002

The alloying elements (Table 9) were not the same, which means it was not the same microalloyed steels that were dealt with in all cases.

Table 10. Chemical composition of Medina's work samples [68]

Steel	C	Si	Mn	Xi	N
Mo1	0.44	0.24	0.79	Mo=0.26	--
Mo2	0.44	0.23	0.79	Mo=0.38	--
Mo3	0.42	0.27	0.79	Mo=0.18	--
T5	0.15	0.24	1.12	Ti=0.021	0.0105
T2	0.15	0.27	1.25	Ti=0.055	0.0100
T3	0.15	0.26	1.10	Ti=0.075	0.0102
V1	0.11	0.24	1.10	V=0.043	0.0105
V2	0.12	0.24	1.10	V=0.060	0.0123
V3	0.11	0.24	1.00	V=0.093	0.0144
N1	0.11	0.24	1.23	Nb=0.041	0.0112
N2	0.11	0.24	1.32	Nb=0.093	0.0119

Medina et al. [68] also proposed a constitutive equation to calculate the hot-working activation energy from their torsion tests and these were also used here for comparison purposes (Figure 50).

The exponent q that shows at which extent the critical strain for DRX depends on the Zener-Hollomon parameter is not influenced by the variation of the soaking temperature. However, as the Nb content was being increased, the value of the exponent q presented two different values that can be considered as two separate regimes.

$$q = \begin{cases} 0.142 \ for \ Nb < 0.068 \\ 0.081 \ for \ Nb \geq 0.068 \end{cases}$$

The appearance of these two regimes could be due to temperature range at which the experiments were conducted. In fact, the compression experiments were supposed to be conducted above the T_{nr} (3.5.4). But for the higher Nb containing steels ($\geq$ 0.068%), it may be that happened that some of the experiments were conducted inadvertently below the T_{NR}.

Table 11. No-recrystallization temperature calculated with Fletcher revised equation [17]

	S5	S4	S3	S2	S1
Nb	0.1	0.068	0.05	0.044	0.0244
T_{NR}	1049	1012	975	972	928

5.5. Retained strain

The retained strain is the amount of strain that remains in a strained steel after it went through a partial softening process (recovery or partial recrystallization). The retained strain was taken into account for the evaluation of the amount of deformation that was necessary to initiate the DRX in the second pass deformation. When the amount of retained strain was high, the critical strain for DRX during the second pass became lower. It can already be noticed that the introduction of a pre-strain promoted the decrease of the deformation needed to initiate DRX (Figure 47).

5.5.1. Influence of deformation temperature on the retained strain

At higher deformation temperatures, the amount of retained strain was lower (Figure 48 and Figure 49), due to higher available driving force or lower thermal activation energy for the softening mechanism during the inter-pass time [63].

5.5.2. Influence of the inter-pass time on the retained strain

From a comparison of the amount of retained strain after 3 seconds of inter-pass time to that after 8 seconds inter-pass time, it was clear that the retained strain from the first pass decreased as the time was made longer between the two hits. It can be noticed that the curves showing the influence on the retained strain shifted down from a shorter inter-pass time to a longer one. A longer time will allow more static rearrangement and restoration [54].

5.6. Effect of Nb content

The addition of Nb increased the hardness, the materials' strength or resistance to deformation (MFS), and the hot working activation energy of the microalloyed steel. It also increased the value of the value of the structural factor A and had a decreasing effect on the austenite grain size, as well as on the softened fraction after the inter-pass time. Interestingly, above 0.068% Nb, no further effect was observed on these properties. The Nb effect is through its carbo-nitride precipitates Nb(C,N) of which there are two types. The first is the fine Nb(C,N) that contributes to the strengthening of the steel by hindering the motion of dislocations and the second type is the coarse Nb(C,N) that is less effective on hindering the dislocation motion [69]. It can be considered that the steel has reached a "ceiling" if it is assumed that beyond 0.068%Nb, no more fine Nb(C,N) is precipitating, only the coarse precipitate's amount is increasing but with no further effect on the properties.

5.7.   Validation of the model

A comparison (Figure 51) was made between the experimental and the predicted values of the critical strain for the onset of dynamic recrystallization for a single pass (compression). A good match was observed between the two sets of values.
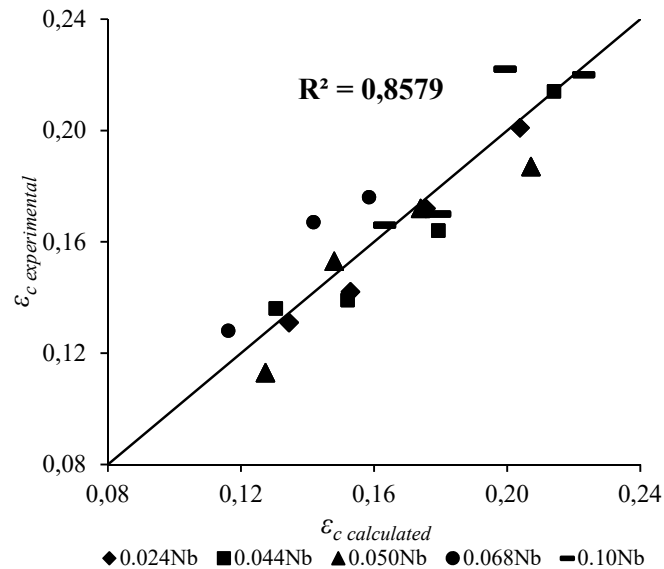
Figure 51. Accuracy of prediction of the critical strain for the onset of DRX for a single pass in Nb-containing HSLA steels

A similar comparison (Figure 52) was made between the experimental values of the retained strain and those that were predicted by the developed equation. A breakdown in the comparison relationship is noticed where $\varepsilon_{r\ calc} > 0.15$; above this amount of retained strain, the function seems not to depend anymore on Nb content because all five steels have data points that are in a deviation referring to the comparison relationship.
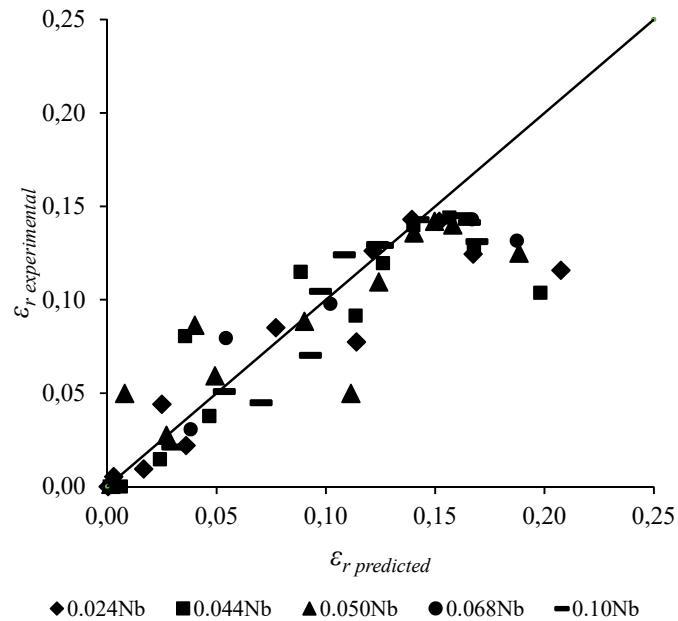
Figure 52. Accuracy of the prediction of the retained strain after a pre-deformation of $\varepsilon \approx 0.142$

Finally, the predicted values of critical strain for the onset of DRX after the introduction of pre-deformation, was compared to the ones experimentally measured (Figure 53). Here again a good match was observed.
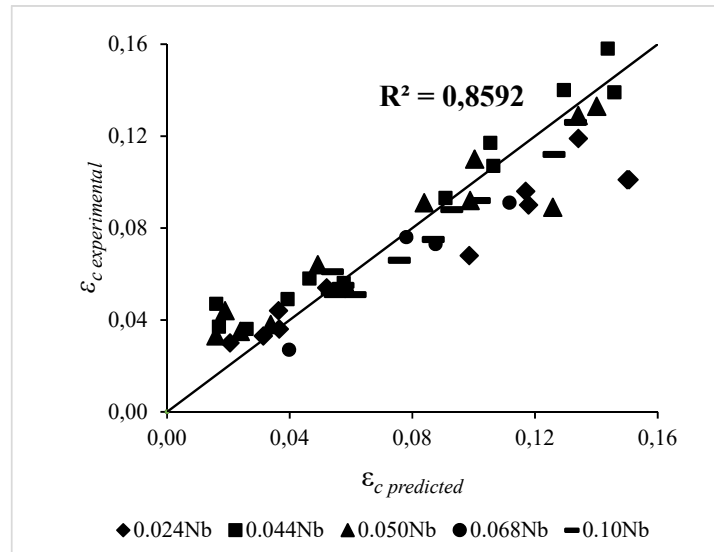
Figure 53. Accuracy of the prediction of the critical strain for the DRX initiation taking into account the retained strain (after a pre-strain).

6. CONCLUSION, INDUSTRIAL RELEVANCE AND FURTHER WORK

6.1. Conclusion

In this work, a pre-deformation was applied to microalloyed steels and it was found that this decreased the amount of strain required to initiate dynamic recrystallization during the subsequent pass. An equation has been developed to calculate the amount of strain that is needed to initiate the dynamic recrystallization during hot-rolling (roughing) of microalloyed Nb-Ti-containing steels, taking into account the retained strain. A good match was observed between the experimental values and those calculated by the developed constitutive equation. A closer look at hot-working experimental results led to the following conclusions:

- Mechanical properties (material's strength, hardness, resistance to hot deformation or mean flow stress, hot working activation energy) were increased by Nb addition but no further effect was observed beyond a "ceiling" of 0.068%Nb.

- A constitutive equation for the calculation of the critical strain for the initiation of DRX (Equation 83) was developed for a single-pass deformation and a further refinement was developed for the prediction of the effect of the retained strain (Equation 85) that remains after a pre-deformation and an inter-pass time at a certain temperature. These two equations were combined to predict the amount of strain required for the initiation of dynamic recrystallization, considering the effect of a pre-strain (Equation 87).

6.2. Industrial relevance

The industrial implications of this work rely on the chemical composition of the steels, the inter-pass times and the amount of deformation per pass.

- The chemical composition is a major component in the design of HSLA steels. The mechanical properties of the product are improved by increasing the Nb content up to a "ceiling" of about 0.07%. Above this amount, the addition of further Nb becomes ineffective.

- A shorter inter-pass time between passes promotes more retention of strain which leads to an earlier dynamic recrystallization. Consequently, a short inter-pass time results in an earlier onset of DRX, which in turn will promote more grain refinement. On the other hand, a shorter inter-pass time will also increase the rate of through put.

- Repeated DRX during the roughing process is needed for grain refinement, therefore the strain of each pass should be greater than the critical strain for the initiation of DRX

6.3.   Further work

Recommendation for further work is as follows:

- For this work, a double-hit compression method was used to evaluate the impact of the initial strain on the critical strain for the onset of DRX in the subsequent pass. More initial passes in the area above T_{NR} can be conducted in order to evaluate the effect on further rolling passes, as the roughing is usually done through 6 to 8 rolling passes.

References

[1] G. R. Ebrahimi, H. Arabshahi and M. Javdani, "Hot deformation behavior of Nb-V microalloyed steel," *Journal of Mechanical Engineering Research,* vol. 2, no. 5, pp. 92-92, 2010.

[2] H. Mohrbacher, "Niobium microalloyed automotive sheet steel - A cost effective solution to the challenge of modern body engineering," in *International Symposium in Microalloyed Sheet steel for Automotive Application, Niobium Products Company GmbH*, Dusseldorf, 2006.

[3] D. Bhattacharya, "Microalloyed steels for the aotomotive industry," *Technol. Metal. Mater. Miner.,* vol. II, no. 4, pp. 371-383, 2014.

[4] S. Vervynckt, K. Verbenken, P. Thibaux, M. Liebeherr and Y. Houbaert, "Austenite Recrystallization-Precipitation Interaction in Niobium Microalloyed Steels," *ISIJ International,* vol. 49, no. 6, pp. 911-920, 2009.

[5] D. A. Skobir, "High-Strength Low-Alloy (HSLA) Steels," *Materials and Technology,* vol. 45, no. 4, pp. 295-301, 2011.

[6] F. J. Siciliano and J. J. Jonas, "Mathematical Modeling of Hot Strip Rolling of Microallyed Nb, Multipy-Alloyed Cr-Mo, and Plain C-Mn Steels," *Metallurgical and Materials Transactions A,* vol. 31 A, pp. 511-530, 2000.

[7] R. Fabik, T. Kbina, S. Aksenov, K. Drodz, I. Schindler and J. Kliber, "Verification of the new model for calculation of critucal strain for the initiation of the dynamic recrystallization using laboratory rolling," *Metallurgija,* pp. 273-276, 2009.

[8] Yun Bo Xu, Yong Mei Yu, Bao Liang Xiao, Zhen Yu Liu and Guo Dong Wang, "Modeling of microstructure evolution during hot rolling of high-Nb HSLA steel," *J Mater Sci,* vol. 45, pp. 2580-2590, 2010.

[9] J. Lu, O. Omotoso, J. B. Wiskel, D. G. Ivey and H. Heinein, "Strengthening Mechanisms and Their Relative Contributions to the Yield Strength of Microalloyed Steels," *Metallurgical and Materials Transactions A,* vol. 43 A, pp. 3043-3061, 2012.

[10] Q. Guo-Zheng, "Characterization for Dynamic Recrystallization Kinetics Based on Stress-Strain Curves," *INTECH,* pp. 61-88, 2013.

[11] "Alloying: Understand the Basics, High-Strength Low-Alloy Steels," *Carbon and Alloy Steels, ASM International,* pp. 193-202, 2001.

[12] S. V. Subramanian, H. S. Zurob and G. Zhu, "Recrystallization control to obtain uniform fine grain size in hot rolling of HTP steels," Department of Materials Science and Engineering, McMaster University, Hamilton.

[13] M. G. Akben, "Precipitation, Recrystallization and Solute strengthening in Microalloyed steels," Department of Mining and Metallurgical Engineering, McGill University, Montreal, 1980.

[14] V. R. Mattes, "Microstructure and mechanical properties of HSLA-100 steel," Naval Postgraduate School, Monterey, California, 1990.

[15] S. H. M. Anijdan, A. Rezaeian and S. Yue, "The effect of chemical composition and austenite conditioning on the transformation behavior of microalloyed steels," *Materials Characterization,* vol. 63, pp. 27-38, 2012.

[16] "High Strength Low Alloy Steels," *ASM Internationl, Carbon and Alloy Steels,* pp. 193-202, 2001.

[17] C. N. Homsher, "Determination of the non-recrystallization temperature (Tnr) in multiple microalloyed steels," Metallurgical and Materials Engineering, Colorado School of Mines.

[18] M. Kashif Ur Rehman, "Modeling the microstructure evolution during hot deformation of microalloyed steels," McMaster University, Hamilton, Ontario, 2014.

[19] Arcelor Mittal South Africa, [Online]. Available: http://southafrica.arcelormittalsa.com/Portals/0/Intro%20to%20Vanderbijlpark%20Works.pdf. [Accessed 14 October 2016].

[20] K. A. Annan, "Effect of Hot Working Characteristics on the Texture Development in AISI 430 and 433 Ferritic Stainless Steel," Department of Materials Science and Metallurgical Engineering, University of Pretoria, 2012.

[21] L. Bäcke, "Modeling the Microstructural Evolution during Hot Deformation of Microalloyed Steels," Universitetsservice US-AB, Stockholm, Sverige, 2009.

[22] J. Biglou, "Dynamic Recrystallization during Strip Rolling of HSLA Steels and Prediction of Roll Forces using Artificial Neural Networks," University of Waterloo, Ontario, 1997.

[23] A. Yoshie, T. Fujita, M. Fujioka, K. Okamoto and H. Morikawa, "Formulation of the Decrease in Dislocation Density of Deformed Austenite Due to Static Recovery and Recrystallization," *ISIJ International,* vol. 36, no. 4, pp. 474-480, 1996.

[24] T. Sakai, A. Belyakov, R. Kaibyshev, H. Miura and J. J. Jonas, "Dynamic and post-dynamic recrystallization under hot, cold and severe plastic deformation conditions," *Progress in Materials Science 60,* pp. 130-207, 2014.

[25] W. E. Stumpf, Phase transformations in metals and their alloys, Course materials for NFM700, University of Pretoria, 2014.

[26] W. E. Stumpf, Basic Physical Metallurgy, Materials Science and Metallurgical Engineering, University of Pretoria, 2014.

[27] R. Nkoma, "Hot Working Characteristics of AISI321 in comparison to AISI 304 austenitic stainless steels," Departement of Materials Science and Metallurical Engineering, University of Pretoria, Pretoria, 2014.

[28] M. Shaban and B. Eghbali, "Characterization of Austenite Dynamic Recrystallization under Different Z Parameters in Microalloyed Steel," *Journal of Materials Science and Technology,* vol. 27, no. 4, pp. 359-363, 2011.

[29] G. A. Guerrero, I. M. Granados and J. M. C. Marrero, "Determination of the critical parameters for the onset of dynamic recrystallization (DRX) in advanced Ultra-High Strength Steels (A-UHSS) microalloyed with boron," *Computer Methods in Materials Science,* vol. 12, no. 3, pp.

152-162, 2012.

[30] S. Solhjoo, "Determination of critical strain for initiation of dynamic recrystallization," *Materials and Design 31,* pp. 1360-1364, 2010.

[31] C. W. Siyasiya and W. E. Stumpf, "Constitutive Constants for Hot Working of Steels: The Critical Strain for Dynamic Recrystallisation in C-Mn Steels," *Journal of Materials Engineering and Performance,* vol. 24, no. I, pp. 468-476, 2015.

[32] E. I. Poliak and J. J. Jonas, "Initiation of Dynamic Recrystallization in Constant Strain Rate Hot Deformation," *ISIJ International,* vol. 43, no. 5, pp. 684-691, 2003.

[33] E. I. Poliak and J. J. Jonas, "Critical Strain for Dynamic Recrystallization in Variable Strain Rate Hot Deformation," *ISIJ International,* vol. 43, no. 5, pp. 692-700, 2003.

[34] L. MA, Z. LIU, S. JIAO, X. YUAN and D. WU, "Dynamic Recrystallization Behaviour of Nb-Ti Microalloyed Steels," *Journal of Wuhan University of Technology - Mater Sci,* pp. 551-557, 2008.

[35] S. Solhojoo and E. Ebrahimi, "Prediction of no-recrystallization temperature by simulation of multi-pass flow stress curves from single-pass cruves," *J Mater Sci,* vol. 45, pp. 5960-5966, 2010.

[36] S. Vervynckt, K. Verbeken, B. Lopez and J. J. Jonas, "Modern HSLA steels and role of non-recrystallisation temperature," *International Materials Reviews,* vol. 57, no. 4, pp. 187-207, 2012.

[37] P. Kumar Ray, R. I. Ganguly and A. K. Panda, "Determination of Recrystallization Stop Temperature (TR) of an HSLA Steel," *Journal of Steel and Related Materials,* no. 5, 2004.

[38] C. Y. Chen, H. W. Yen, F. H. Kao, W. C. Li, C. Y. Huang, J. R. Yang and S. H. Wang, "Precipitation hardening of high-strength low-alloy steels by nanometer-sized carbides," *Materials Science and Engineering A,* no. 499, pp. 162-166, 2009.

[39] S. Shanmugam, M. Tanniru, R. D. K. Misra, D. Panda and S. Jansto, "Microalloyed V-Nb-Ti and V steels Part 2 - Precipitation behaviour during processing of structural beams," *Materials Science and Technology,* vol. 21, no. 2, pp. 165-177, 2005.

[40] G. Krauss, Steels-Processing, Structure, and Performance, Colorado: ASM International, 2005.

[41] Y. Lu, "Effect of Boron on Microstructure and Mechanical Properties of of Low Carbon Microalloyed Steels," Library and Archives, McGill University, Montreal, 2007.

[42] L. Backe, "Modeling the Microstructural Evolution during Hot Deformation of Microalloyed steels," Universitetsservice US-AB, Stockholm, Sveridge, 2009.

[43] S. F. Medina and C. A. Hernandez, "The influence of chemical composition on peak strain of deformed austenite in Low Alloy and Microalloyed Steels," *Acta Metallurgica,* vol. 44, no. 1, pp. 149-154, 1996.

[44] M. G. Akben, I. Weiss and J. J. Jonas, "Dynamic Precipitation and Solute hardening in a V Microalloyed Steel and two Nb Steels Containing High level of Mn," *Acta Metallurgica,* vol. 29,

pp. 111-121, 1980.

[45] F. A. Burgmann, Y. Xie, J. M. Cairney, S. P. Ringer, C. R. Killmore, F. J. Barboro and J. G. Williams, "The effect of Niobium additions on ferrite formation in CASTRIP Steel," *Materials Forum,* vol. 32, pp. 9-12, 2008.

[46] H.-l. Wei and G.-q. Liu, "Effect of Nb and C on the hot flow behavior of Nb microalloyed steels," *Materials and Design,* vol. 56, pp. 437-444, 2014.

[47] M. Gomez and S. F. Medina, "Role of Microalloying Elements on the Microstructure of Hot Rolled Steels," *International Journal of Materials Research,* vol. 102, pp. 1197-1207, 2011.

[48] K. M. Banks, A. Tuling and B. Mintz, "Influence of V and Ti on hot ductility of Nb containing of peritectic C contents," *Materials Science and Technology,* vol. 27, no. 8, pp. 1309-1314, 2011.

[49] J. Fang, "Study on the Mechanism of Strengthning and Toughening Effect of Titanium Addition on HSLA Steel," Technology Center, Shanghai China.

[50] C. Roucoules, S. Yue and J. J. Jonas, "Effect of Alloying Elements on Metadynamic Recristallization in HSLA Steels," *Metallurgical and Materials Transactions A,* vol. 26A, pp. 181-190, 1995.

[51] C. Grade Andres, M. J. Bartolome, C. Capdevila, D. San Martin, F. G. Caballero and V. Lopez, "Metallographic techniques for the determination of the austenite grain size in medium-carbon microalloyed steels," Department of Physical Metallurgy, Centro Nacional de Investigaciones Metalurgicas (CENIM), Madrid, 2001.

[52] K. Banerjee, M. Militzer, M. Perez and W. Xiang, "Nonisothermal Grain Growth Kinetics in Microalloyed X80 Linepipe Steel," *Metallurgical and Materials A,* vol. 41A, no. 12, pp. 3161-3172, 2010.

[53] A. V. Chastukhin, D. A. Ringinen, G. E. Khadeev and L. I. Efron, "Kinetics of static recrystallization of austenite in Nb microalloyed pipe steels," *Mettalurgist,* vol. 59, no. 11, pp. 1180-1187, 2016.

[54] A. Najafi-Zadeh and R. Ebrahimi, "Effect of Delay Time on Microstructural Evolution during Warm Rolling of Ti-Nb-IF steel," *J. Mater. Sci. Technol,* vol. 20, no. 1, pp. 86-88, 2004.

[55] R. C. K. Nkoma, C. W. Siyasiya and W. E. Stumpf, "Hot workability of AISI 321 and AISI 304 austenitic stainless steels," *Journal of Alloys and Compounds,* no. 595, pp. 103-112, 2014.

[56] F. J. Siciliano, "Mathematical Modeling of the Hot Strip Rolling of Nb Microalloyed Steels," National Library of Canada, Montreal, Canada, 1999.

[57] F. Alghamdi, "Mathematical Modeling of Mean Flow Stress (MFS) during Hot Strip Rolling fro HSLA Steels," McGill University, Montreal, Canada, 2013.

[58] C. Gracia-Mateo, B. Lopez and J. M. Rodriguez-Ibade, "Static recrystallization kinetics in warm worked vanadium microalloyed steels," *Materials Science and Engineering A,* no. 303, pp. 216-225, 2001.

[59] M. Opiela and W. Ozgowicz, "Effects of Nb, Ti and V on recrystallization kinetics of austenite

in microalloyed steels," *Journal of Achievement in Materials and Manufacturing Engineering,* vol. 55, no. 2, pp. 759-771, 2012.

[60] A. V. Chastukhin, D. A. Ringinen, G. E. Khadeev and L. I. Efron, "Kinetics of static recrystallization of austenite in Niobium-Microalloyed pipe steels," *Metallurgist,* vol. 59, pp. 1180-1187, 2016.

[61] D. Houghton, "Equilibrium solubility and Composition of mixed carbonitrides in microalloyed austenite," *Acta Metall. Mater. ,* vol. 41, no. 10, pp. 2993-3006, 1993.

[62] J. Speer, J. Michael and S. Hansen, "Carbonitride Precipitation in Niobium/Vanadium Microalloyed Steels," *Metallurgical Transactions A,* vol. 18A, pp. 211-222, 1987.

[63] X.-d. HUO, X.-p. MAO and S.-x. LU, "Effect of Annealing Temperature on Recrystallization Behavior of Cold Rolled Ti-Microalloyed Steel," *Journal of Iron and Steel Research, International,* vol. 20, no. 9, pp. 105-110, 2013.

[64] S. F. Medina, M. Gomez, E. Rodriguez and L. Rancel, "Influence of Accumulated Stress in Austenite on the Transformed Ferrite Grain Size by Hot Rolling for a V-microalloyed Steel," *ISIJ International ,* vol. 48, no. 9, pp. 1263-1269, 2008.

[65] B.-B. Jung, H.-K. Lee and H.-C. Park, "Effect of grain size on the indentation hardness for polycrystalline materials by the modified strain gradient theory," *International Journal of Solids and Structures,* no. 50, pp. 2719-2724, 2013.

[66] M. Hakamada, Y. Nakamoto, H. Matsumoto, H. Iwasaki, Y. Chen, H. Kusuda and M. Mabuchi, "Relationship between hardness and grain size in electrodeposited copper films," *Materials Science and Engineering A,* no. 457, pp. 120-126, 2007.

[67] S. F. Medina and C. A. Hernandez, "General expression of the Zener-Hollomon parameter as a function of the chemical compostion of Low Alloy and Microalloyed Steels," *Acta Materialia,* vol. 44, no. 1, pp. 137-148, 1996.

[68] S. F. Medina and C. A. Hernandez, "General expression of the Zener-Hollomon parameter as a function of the chemical composition of Low Alloy and Microalloyed Steels," *Acta Materialia,* vol. 44, no. 1, pp. 137-148, 1996.

[69] O. Takashi, W. Takashi, A. Masanori and A. Kazumi, "Effect of V and Nb on precipitation behavior and mechanical properties of high Cr steel," *Nuclear Engineering and Design,* vol. 238, no. 2, pp. 408-416, 2008.

[70] W. Stumpf, "Mechanichal Metallurgy NMM700," Pretoria, 2014.

[71] L. M. Fu, H. R. Wang, W. Wang and A. D. Shan, "Austenite grain growth prediction coupling with drag and pinning effects in low carbon Nb microalloyed steels," *Materials Science and Technology,* vol. 27, no. 6, pp. 996-1001, 2011.

[72] A. Kostryzhev, A. A. Shahrani, C. Zhu, S. P. Ringer and E. V. Pereloma, "Effect of austenitizing and deformation temperature on dynamic recrystallisation in Nb-Ti microalloyed steel," *Materials Science Forum,* vol. 753, pp. 431-434, 2013.

[73] C. G. Andres, M. J. Bartolome, C. Capdevila, D. San Martin, F. G. Caballero and V. Lopez,

"Metallographic techniques for the determination of the austenite grain size in medium-carbon microalloyed steels," Madrid, 2001.

[74] S. Maropoulos, S. Karagiannis and N. Ridley, "The effect of austenitising temperature on prior austenite grain size in a low-alloy steel," *Materials Science and Engineering A,* no. 483-483, pp. 735-739, 2008.

[75] A. S. Kumar, B. R. Kumar, G. Datta and V. Ranganath, "Effect of microstructure and grain size on the fracture toughness of a micro-alloyed steel," *Materials Science and Engineering A,* no. 527, pp. 954-960, 2010.

[76] W. Stumpf, "Grain size modelling of a low carbon strip steel during hot rolling in a Compact Strip Production (CSP) plant using the Hot Charge Route," *The Journal of The South African Institute of Mining and Metallurgy,* vol. 103, no. 10, pp. 617-631, 2003.

APPENDICES

Table 12. Effect of deformation temperature, inter-pass time and chemical composition on the retained strain

ID	Nb%	T	ε_i	t_{ip}	ε_r pred.	ε_r exp.
S1	0.024	1273	0.142	0.5	0.152	0.142
S1	0.024	1323	0.143	0.5	0.139	0.143
S1	0.024	1373	0.137	0.5	0.122	0.126
S1	0.024	1423	0.141	0.5	0.114	0.077
S1	0.024	1273	0.141	3	0.167	0.124
S1	0.024	1323	0.141	3	0.077	0.085
S1	0.024	1373	0.143	3	0.036	0.022
S1	0.024	1423	0.143	3	0.017	0.009
S1	0.024	1323	0.145	8	0.025	0.044
S1	0.024	1373	0.142	8	0.003	0.005
S1	0.024	1423	0.142	8	0.000	0.000
S5	0.10	1273	0.142	0.5	0.162	0.145
S5	0.10	1323	0.143	0.5	0.142	0.143
S5	0.10	1373	0.145	0.5	0.126	0.129
S5	0.10	1423	0.143	0.5	0.108	0.124
S5	0.10	1273	0.142	3	0.166	0.141
S5	0.10	1323	0.141	3	0.124	0.130
S5	0.10	1373	0.141	3	0.093	0.070
S5	0.10	1423	0.142	3	0.070	0.045
S5	0.10	1273	0.138	8	0.169	0.131
S5	0.10	1323	0.143	8	0.098	0.105
S5	0.10	1373	0.141	8	0.054	0.051
S5	0.10	1423	0.142	8	0.030	0.021

Table 13. Effect of deformation temperature, strain rate, retained strain and inter-pass time on the critical strain for DRX initiation.

ID	Nb%	T	$\dot{\varepsilon}$	ε_c calc.	ε_c exper.	ε_i	t_{ip}	ε_r calc.	ε_r exp.	ε_{ci+1} calc.	ε_{ci+1} exper.
S1	0.024	1273	0.44	0.207	0.187	0.142	0.5	0.152	0.142	0.052	0.054
S1	0.024	1323	0.44	0.174	0.172	0.143	0.5	0.139	0.143	0.036	0.044
S1	0.024	1373	0.44	0.148	0.153	0.137	0.5	0.122	0.126	0.031	0.033
S1	0.024	1423	0.44	0.127	0.113	0.141	0.5	0.114	0.077	0.021	0.030
S1	0.024	1273	0.44	0.207	0.187	0.141	3	0.167	0.124	0.037	0.036
S1	0.024	1323	0.44	0.174	0.172	0.141	3	0.077	0.085	0.099	0.068
S1	0.024	1373	0.44	0.148	0.153	0.143	3	0.036	0.022	0.117	0.096
S1	0.024	1423	0.44	0.127	0.113	0.143	3	0.017	0.009	0.118	0.090
S1	0.024	1323	0.44	0.174	0.172	0.145	8	0.025	0.044	0.151	0.101
S1	0.024	1373	0.44	0.148	0.153	0.142	8	0.003	0.005	0.150	0.101
S1	0.024	1423	0.44	0.127	0.113	0.142	8	0.000	0.000	0.134	0.119
S5	0.10	1273	0.44	0.223	0.220	0.142	0.5	0.162	0.145	0.061	0.051
S5	0.10	1323	0.44	0.199	0.222	0.143	0.5	0.142	0.143	0.057	0.052
S5	0.10	1373	0.44	0.180	0.170	0.145	0.5	0.126	0.129	0.054	0.052
S5	0.10	1423	0.44	0.163	0.166	0.143	0.5	0.108	0.124	0.055	0.051
S5	0.10	1273	0.44	0.223	0.220	0.142	3	0.166	0.141	0.057	0.055
S5	0.10	1323	0.44	0.199	0.222	0.141	3	0.124	0.130	0.076	0.066
S5	0.10	1373	0.44	0.180	0.170	0.141	3	0.093	0.070	0.087	0.075
S5	0.10	1423	0.44	0.163	0.166	0.142	3	0.070	0.045	0.093	0.088
S5	0.10	1273	0.44	0.223	0.220	0.138	8	0.169	0.131	0.054	0.061
S5	0.10	1323	0.44	0.199	0.222	0.143	8	0.098	0.105	0.102	0.092
S5	0.10	1373	0.44	0.180	0.170	0.141	8	0.054	0.051	0.126	0.112
S5	0.10	1423	0.44	0.163	0.166	0.142	8	0.030	0.021	0.133	0.126

*Table 14. Excel sheet template used for the flow curves generation*

| Exp/series no:	S2	Material:		HSLA steel	Cast/slab no	NA	Condition:	Hot rolled	Test date	07/09/2015		
Main purpose	Constitutive constants		Initial sample	D(0) cold mm	H(0) cold mm	D(0) hot mm	H(0) hot mm					
of test	for Hot Working		dimensions	4.992	10.003	5.061	10.142					
Heat up to 1200C in 15 min, soak for 10 min			Final sample	D(f) cold mm	H(f) cold mm	D(f) hot mm	H(f) hot mm					
Lower to 1100C for deformation, slowly cooled			dimensions	9.3	3.15	9.429	3.194					
		Plan'd def t	1.5	Actual stroke	-5.208	Barrel factor	0.915					
Gleeble prg		Act def time	1.600	Plan'd strain	0.65	Plan'd str rte	0.5					
Load cell	1.000	Plan'd def T	1050	Actual strain	0.720	Calc str rte	0.450					
Corr factor	NA	Meas def T	1100.0	Meas cold str	1.155	Cold str rt	0.722					
Gleeble prg data point	Gleeble time seconds	Temp. meas. Deg C	Gleeble stroke mm	Gleeble force kN	Zero'd Gleeble stroke mm	Zero'd Gleeble force N	True strain (negative)	Flow stress (no friction) MPa	Von Mises flow stress (fr=0.2) MPa	Cum stress/ strain (no friction)	Cum stress/ strain (fr=0.2)
---	---	---	---	---	---	---	---	---	---	---	---
0	1531.05	1100	-0.00045748	-0.86939	0.0000	0.00	0.000	0.0	0.0	0.00	0.00
1	1531.06	1100	0.00025261	-0.91047	0.0007	41.08	0.000	2.0	2.0	0.00	0.00
2	1531.07	1100	0.00054865	-0.93723	0.0010	67.84	0.000	3.4	3.3	0.00	0.00
3	1531.08	1100	-0.0036076	-1.1116	-0.0032	242.21	0.000	12.0	11.8	0.01	0.01
4	1531.09	1100	-0.010543	-1.2861	-0.0101	416.71	0.001	20.7	20.3	0.07	0.07
5	1531.1	1100	-0.031214	-1.4818	-0.0308	612.41	0.003	30.3	29.8	0.22	0.22
6	1531.11	1100	-0.080619	-1.5432	-0.0802	673.81	0.008	33.2	32.7	0.45	0.44
7	1531.12	1100	-0.14433	-1.6726	-0.1439	803.21	0.014	39.4	38.7	0.73	0.71
8	1531.13	1100	-0.2114	-1.7341	-0.2109	864.71	0.021	42.1	41.4	1.03	1.01
9	1531.14	1100	-0.27832	-1.8647	-0.2779	995.31	0.028	48.1	47.3	1.34	1.32
10	1531.15	1100	-0.3402	-1.8983	-0.3397	1028.91	0.034	49.4	48.6	1.57	1.55
11	1531.16	1100	-0.38534	-1.9774	-0.3849	1108.01	0.039	53.0	52.0	1.75	1.72
12	1531.17	1100	-0.41735	-1.945	-0.4169	1075.61	0.042	51.3	50.4	1.88	1.84
13	1531.18	1100	-0.44153	-1.9834	-0.4411	1114.01	0.044	53.0	52.0	1.98	1.95
14	1531.19	1100	-0.46185	-1.9441	-0.4614	1074.71	0.047	51.0	50.1	2.09	2.06
15	1531.2	1100	-0.48218	-1.9706	-0.4817	1101.21	0.049	52.1	51.2	2.20	2.16
16	1531.21	1100	-0.5021	-1.9371	-0.5016	1067.71	0.051	50.4	49.5	2.31	2.27
17	1531.22	1100	-0.5223	-1.9776	-0.5218	1108.21	0.053	52.2	51.3	2.43	2.38
18	1531.23	1100	-0.54433	-1.9818	-0.5439	1112.41	0.055	52.3	51.4	2.56	2.52
19	1531.24	1100	-0.56838	-2.0687	-0.5679	1199.31	0.058	56.3	55.3	2.75	2.70
20	1531.25	1100	-0.59984	-2.0995	-0.5994	1230.11	0.061	57.5	56.5	2.96	2.90
21	1531.26	1100	-0.63294	-2.1833	-0.6325	1313.91	0.064	61.2	60.1	3.19	3.13
22	1531.27	1100	-0.6694	-2.1735	-0.6689	1304.11	0.068	60.5	59.4	3.44	3.38
23	1531.28	1100	-0.70836	-2.2255	-0.7079	1356.11	0.072	62.7	61.5	3.71	3.64
24	1531.29	1100	-0.74801	-2.199	-0.7476	1329.61	0.077	61.2	60.1	3.97	3.90
25	1531.3	1100	-0.78828	-2.2571	-0.7878	1387.71	0.081	63.6	62.4	4.24	4.17
26	1531.31	1100	-0.82828	-2.2434	-0.8278	1374.01	0.085	62.7	61.5	4.51	4.43
27	1531.32	1100	-0.86656	-2.3268	-0.8661	1457.41	0.089	66.2	65.0	4.79	4.70
28	1531.33	1100	-0.90577	-2.3385	-0.9053	1469.11	0.094	66.5	65.2	5.07	4.98
29	1531.34	1100	-0.9436	-2.4185	-0.9431	1549.11	0.098	69.8	68.5	5.34	5.25
30	1531.35	1100	-0.97981	-2.3983	-0.9794	1528.91	0.102	68.7	67.3	5.61	5.51
31	1531.36	1100	-1.0146	-2.4387	-1.0141	1569.31	0.105	70.2	68.8	5.85	5.74
32	1531.37	1100	-1.0461	-2.398	-1.0456	1528.61	0.109	68.1	66.8	6.09	5.98
33	1531.38	1100	-1.0781	-2.4394	-1.0776	1570.01	0.112	69.7	68.4	6.31	6.19
34	1531.39	1100	-1.1066	-2.4045	-1.1061	1535.11	0.115	68.0	66.6	6.51	6.40
35	1531.4	1100	-1.1339	-2.4472	-1.1334	1577.81	0.119	69.7	68.3	6.74	6.62
36	1531.41	1100	-1.1633	-2.4221	-1.1628	1552.71	0.122	68.3	67.0	6.97	6.84
37	1531.42	1100	-1.1926	-2.4833	-1.1921	1613.91	0.125	70.8	69.4	7.20	7.06
38	1531.43	1100	-1.2215	-2.4786	-1.2210	1609.21	0.128	70.4	68.9	7.43	7.29
39	1531.44	1100	-1.2507	-2.5527	-1.2502	1683.31	0.132	73.3	71.9	7.67	7.53
40	1531.45	1100	-1.2799	-2.5477	-1.2794	1678.31	0.135	72.9	71.4	7.92	7.78
41	1531.46	1100	-1.3099	-2.6119	-1.3094	1742.51	0.138	75.4	73.9	8.18	8.03
42	1531.47	1100	-1.3404	-2.5892	-1.3399	1719.81	0.142	74.2	72.7	8.44	8.28
43	1531.48	1100	-1.3703	-2.6358	-1.3698	1766.41	0.145	75.9	74.4	8.73	8.56
44	1531.49	1100	-1.4041	-2.6021	-1.4036	1732.71	0.149	74.2	72.7	9.02	8.85
45	1531.5	1100	-1.4381	-2.6482	-1.4376	1778.81	0.153	75.9	74.3	9.32	9.15
46	1531.51	1100	-1.4732	-2.6265	-1.4727	1757.11	0.157	74.6	73.1	9.63	9.44
47	1531.52	1100	-1.5079	-2.6804	-1.5074	1811.01	0.161	76.6	75.0	9.93	9.74
48	1531.53	1100	-1.5426	-2.6644	-1.5421	1795.01	0.165	75.6	74.0	10.24	10.04
49	1531.54	1100	-1.5765	-2.7389	-1.5760	1869.51	0.169	78.5	76.8	10.56	10.35
50	1531.55	1100	-1.6111	-2.7454	-1.6106	1876.01	0.173	78.4	76.7	10.89	10.68
51	1531.56	1100	-1.6466	-2.8126	-1.6461	1943.21	0.177	80.9	79.2	11.22	11.00
52	1531.57	1100	-1.6814	-2.796	-1.6809	1926.61	0.181	79.9	78.1	11.55	11.32
53	1531.58	1100	-1.7157	-2.8351	-1.7152	1965.71	0.185	81.2	79.4	11.85	11.61
54	1531.59	1100	-1.7472	-2.8001	-1.7467	1930.71	0.189	79.4	77.7	12.17	11.93
55	1531.6	1100	-1.7815	-2.8327	-1.7810	1963.31	0.193	80.4	78.7	12.50	12.25

S1 1200 °C
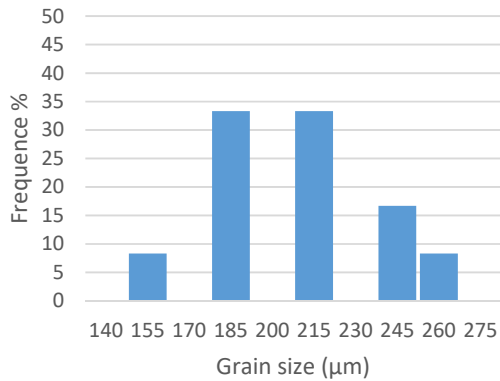
S1 1290 °C
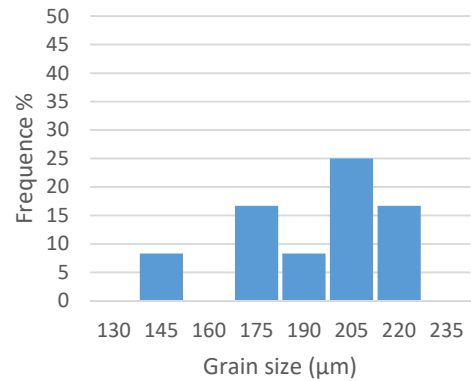
S2 1200 °C
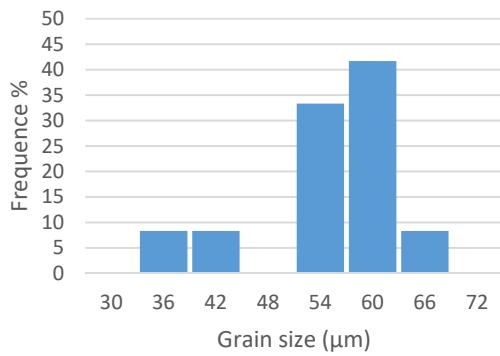
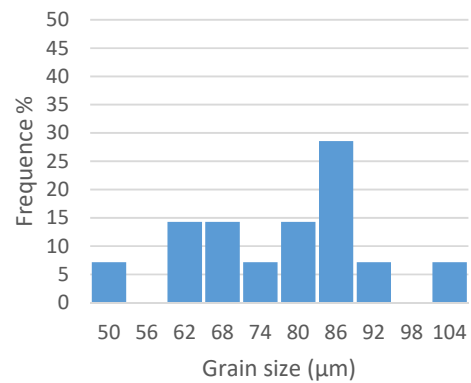### S2 1290 °C

S4 1200 °C

S4 1290 °C

D
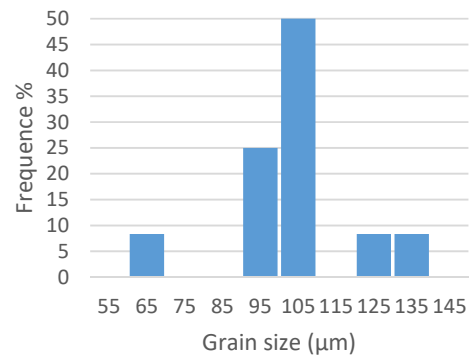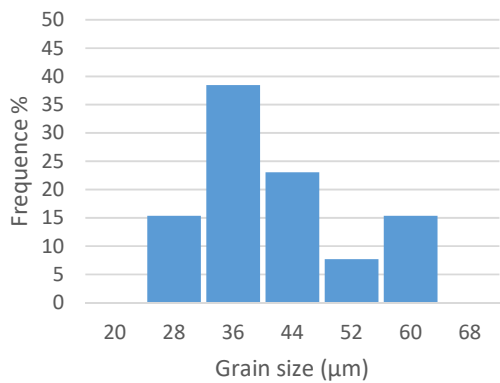
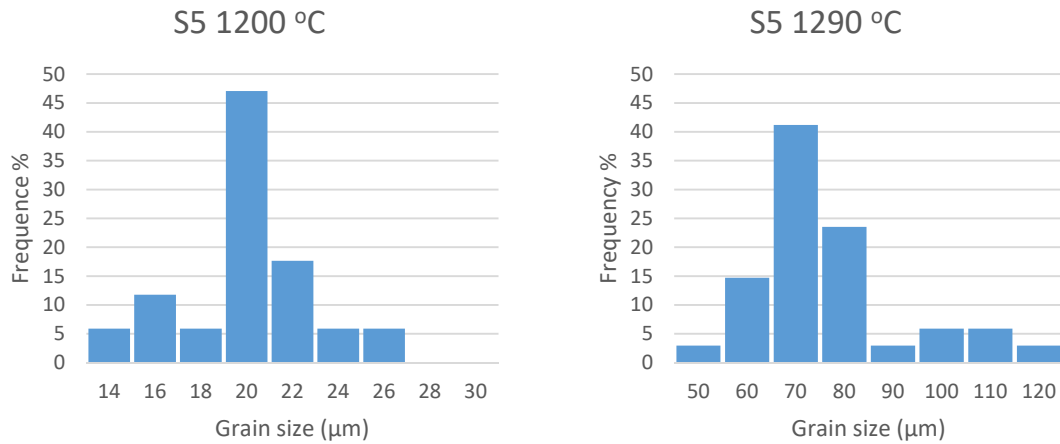## S5 1200 ºC

S5 1290 ºC

Figure 54. Frequency distributions of grain size measured after soaking at 1200 ºC (left) and 1290 ºC (right).

Table 15. Detailed results of grain size measurement

T$_A$		S1	S2	S4	S5
1200 ºC	Median	202	48	39	20
	Average	197	50	38	19
	St. Dev	30	8	10	3
1290 ºC	Median	240	86	75	79
	Average	221	97	74	71
	St. Dev	73	17	15	15